(Please see our responses in blue)

Comments to the Author:

Editor Decision

Dear Dr. Guo,

Thank you for revising the manuscript and providing extensive responses and explanations of the changes. You have addressed the basic concerns. There remain a few technical issues that should be addressed:

Thank you so much for your consideration, our responses to your questions and corresponding revisions are specified below.

- Fig. S1: The bins for the x-axis are selected such that the figures are not informative (e.g., all TSS observations fall into the same category). Please adapt the scale and bins accordingly.

We have revised Fig. S1 to better visualize the highly skewed data. Specifically, for each constituent the plot only show up to the 99th percentile of all records, and the maximum value is highlighted in the corresponding panel title (see below).

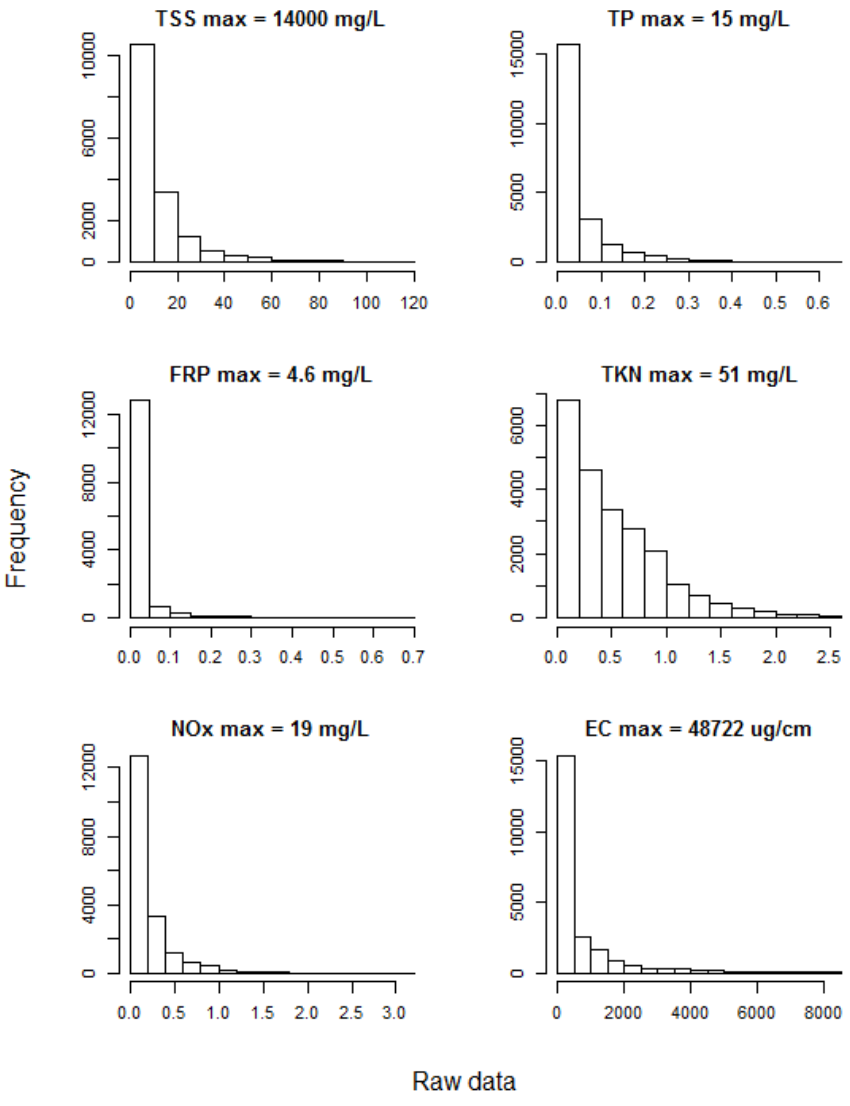

Figure S1. Distribution of the raw water quality data across all catchments. Each panel shows one constituent with only the above-DL data. To help visualizing the highly skewed data, the top percentile of data for each constituent were not plotted, while the maximum value was shown in the corresponding panel title.

- Tab. 5 (and the respective text): For TSS, FRP, NOx the full model performs worse than the minimum of all 50 partial models. Does this not indicate that there is an incompatibility of the data in space and time that cannot fully resolved by the model? Or what is your interpretation? Should this not be briefly mentioned in the text?

Thank you so much for raising this issue. After careful checking of the results, we found that in the previous version of Table 5, the full-model performances were based on only the above-DL data, whereas the performances of the 50 partial models (cross-validation) were based on all (calibration or validation) data including both the above- and below-DL values. So, these two model evaluations were not in comparable scales in the previous manuscript.

During correction we have updated the 'full model performance' in Table 5 with that for all data including the below-DL records (see below), so that the full models NSEs and now more comparable with the cross-validation NSEs.

Table 5. Comparison of model performances (as NSE) of the full model (Column 2) and the 50 partial models (Columns 3 to 5) with each calibrated to 80% randomly selected monitoring sites. Columns 3 to 5 summarize the mean, minimum and maximum NSE values across the 50 runs, where for each constituent, the top row showing calibration performance and the bottom row showing the validation performance (i.e. at the 20% sites that were not used for calibration).

Constituent	Full model	50 CV mean	50 CV min	50 CV max
TSS	0.397	0.413	0.376	0.439
		0.382	0.292	0.513
TP	0.445	0.461	0.427	0.501
		0.411	0.151	0.575
FRP	0.199	0.168	0.067	0.232
		0.129	-0.078	0.272
TKN	0.630	0.654	0.622	0.670
		0.622	0.468	0.691
NO_x	0.382	0.453	0.414	0.489
		0.397	0.258	0.563
EC	0.886	0.893	0.882	0.903
		0.875	0.809	0.924

After this revision, the only result that still needs further attention is for NO_x, where the cross-validation performances are still clearly better than that of the full-model. We think this might be related to differences in the proportions of below-DL data used to evaluate the full model and the partial models. We have presented detailed explanation in the main text as:

- *L471: "Note the slightly higher calibration performance for the partial models of NOx compared to the full model. This seems to be related to the generally lower percentages of below-DL data in the 50 randomly-chosen partial calibration datasets (14.1%-17.9%) compared to the full dataset (17.3%) – we further discuss the impacts of below-DL data on model performance in Section 4.1."*

In consistent with Table 5, the 'full model performance' in Table 6 (which compares the full model performance with the calibration/validation performance of three sub-periods) was also updated with inclusion of the below-DL values. Further, in consistent with these, we have also updated the corresponding model performances summary in the Abstract with inclusion of the below-DL values:

- *L19: "Apart from FRP, which is hardly explainable (19.9%), the model explains 38.2% (NOx) to 88.6% (EC) of total spatio-temporal variability in water quality."*

- Table 6: The caption is wrong (Table 3).

This has been revised.

Sincerely

Christian Stamm

Editor HESS

Again we thank you for your time and effort in handling this manuscript. We believe that the manuscript has been greatly benefited from the review process.

A data-based predictive model for spatio-temporal variability in stream water quality

Danlu Guo[1], Anna Lintern[1,2], J. Angus Webb[1], Dongryeol Ryu[1], Ulrike Bende-Michl[3], Shuci Liu[1], Andrew William Western[1]

[1] Department of Infrastructure Engineering, The University of Melbourne, Parkville, VIC Australia;

[2] Department of Civil Engineering, Monash University, Clayton, VIC Australia

[3] Bureau of Meteorology, Parkes, ACT Australia.

Corresponding author's email: danlu.guo@unimelb.edu.au

Abstract

Our current capacity to model stream water quality is limited particularly at large spatial scales across multiple catchments. To address this, we developed a Bayesian hierarchical statistical model to simulate the spatio-temporal variability in stream water quality across the state of Victoria, Australia. The model was developed using monthly water quality monitoring data over 21 years, across 102 catchments, which span over 130,000 km^2. The modelling focused on six key water quality constituents: total suspended solids (TSS), total phosphorus (TP), filterable reactive phosphorus (FRP), total Kjeldahl nitrogen (TKN), nitrate-nitrite (NO_x), and electrical conductivity (EC). The model structure was informed by knowledge of the key factors driving water quality variation, which had been identified in two preceding studies using the same dataset. Apart from FRP, which is ~~largely un~~hardly explainable (19.9%), the model explains ~~21.~~38.2~~6~~% (NO_x) to ~~90.7~~88.6% (EC) of total spatio-temporal variability in water quality. Across constituents, the model generally captures over half of the observed spatial variability; temporal variability remains largely unexplained across all catchments, while long-term trends are well captured. The model is best used to predict proportional changes in water quality in a Box-Cox transformed scale, but can have substantial bias if used to predict absolute values for high concentrations. This model can assist catchment management by (1) identifying hot-spots and hot moments for waterway pollution; (2) predicting effects of catchment changes on water quality e.g. urbanization or forestation; and (3) identifying and explaining major water quality trends and changes. Further model improvements should focus on: (1) alternative statistical model structures to improve fitting for truncated data, for constituents where a large amount of data below the detection-limit; and (2) better representation of non-conservative constituents (e.g. FRP) by accounting for important biogeochemical processes.

Keywords

stream water quality; spatio-temporal variability; sediments; nutrients; statistical modeling; Bayesian hierarchical model

1. Introduction

Deteriorating water quality in aquatic systems such as rivers and streams can have significant environmental, economic and social ramifications (e.g. Whitworth et al., 2012;Vörösmarty et al., 2010;Qin et al., 2010;Kingsford et al., 2011). Reducing these impacts requires effective management and mitigation of poor water quality; however, high variability in water quality both across space and time reduces our ability to accurately assess the status of water quality and to develop effective management strategies. Thus, improved modelling frameworks to predict and interpret this variability would be useful for water quality management (Chang, 2008;Ai et al., 2015;Zhou et al., 2012).

Water quality conditions can vary across individual events, as well as at daily, seasonal and inter-annual scales at an individual location (Arheimer and Lidén, 2000; Kirchner et al., 2004; Larned et al., 2004; Pellerin et al., 2012; Saraceno et al., 2009). Water quality conditions also typically differ substantially across locations (Meybeck and Helmer, 1989;Chang, 2008;Varanka et al., 2015;Lintern et al., 2018a). These variabilities in stream water quality are driven by three key mechanisms: (1) source, which defines the total amount of constituents being available in a catchment; (2) mobilization, which detaches constituents (both in particulate and dissolved forms) from their sources via processes such as erosion and biogeochemical processing; and (3) delivery of mobilized constituents from catchments to receiving waters via multiple hydrologic pathways including surface and subsurface flow (Granger et al., 2010).

Spatial variability in stream water quality is driven by human activities within catchments (e.g., land use and management, vegetation cover etc.) (Lintern et al., 2018a;Carey and Migliaccio, 2009;Giri and Qiu, 2016;Heathwaite, 2010), along with natural catchment characteristics such as climate, geology, soil type, topography and hydrology (Hrachowitz et al., 2016;Poulsen et al., 2006;Sueker et al., 2001;Onderka et al., 2012). At the same time, temporal shifts in water quality are also influenced by changes in pollutant sources, such as land use and land management including urbanization, agriculture and vegetation clearing (Ren et al., 2003;Smith et al., 2013;Ouyang et al., 2010). In addition, water quality can also vary in time with variations in the mobilization and delivery processes, which are largely driven by the hydro-climatic conditions at a catchment, such as streamflow (Ahearn et al., 2004;Mellander et al., 2015;Sharpley et al., 2002;Zhang and Ball, 2017), the timing and magnitude of rainfall events (Fraser et al., 1999;Miller et al., 2014) and temperature (Bailey and Ahmadi, 2014).

As abovementioned, we have good understanding of the key controls for variations in water quality, albeit in an isolated, idealized context. We still lack a sound understanding of how relationships between specific landscape characteristics and water quality can shift with influences from other landscape characteristics, and how the drivers of temporal variability in water quality can interact and vary across large spatial scales (Musolff et al., 2015;Lintern et al., 2018a;Ali et al., 2017). In contrast, current detailed understanding have been primarily based on field studies at small scales with detailed information on specific temporal drivers ranging from hydrologic conditions to detailed management decisions such as fertilizer rates and application timing (Smith et al., 2013;Poudel et al., 2013;Adams et al., 2014). While operational weather observation networks, stream gauging networks and remote sensing can provide some of this information, developing a large-scale understanding of water quality patterns across catchments would ideally also involve an extensive suite of management information that substantially exceeds what is currently available.

Due to the limited understanding of large-scale water quality patterns, we currently lack the capacity to model spatio-temporal variabilities in water quality at large scales across multiple catchments. This hinders our ability to inform the development of effective policy and mitigation strategies over large regions. Specifically, conceptual or physically-based water quality models are typically limited by the simplification of physical processes such as flow pathways (Hrachowitz et al., 2016). Furthermore, practical implementation of these models can be also limited by the intensive data requirements for calibration and validation, particularly for large regions with highly heterogeneous catchment conditions (Fu et al., 2018;Abbaspour et al., 2015). In contrast, when performed over large geographical regions, statistical water quality models are generally more capable of simulating water quality variability while requiring less detailed information and thus effort for implementation. However, existing statistical models often focus only on either the spatial variation of time-averaged water quality conditions (Tramblay et al., 2010;Ai et al., 2015) or the temporal variation at individual locations (Kisi and Parmar, 2016;Kurunç et al., 2005;Parmar and Bhardwaj, 2015), which often limits their value as practical management tools. Modelling the spatio-temporal variability simultaneously remains challenging over long time periods and large regions.

Accordingly, this research attempts to bridge the gap between fully-distributed physically-based water

quality models and data-driven statistical approaches. We aim to develop a process-informed, data-driven model to predict spatio-temporal changes in stream water quality over a large region consisting of multiple catchments. Specifically, this model was established using long-term (21 years) stream water quality observations across 102 catchments in Australia, with an aggregate catchment area of 130,000 km^2. To obtain the necessary understanding of process drivers required to develop this model, two preceding studies were conducted on the same dataset to identify the key drivers for the spatial and temporal variability of water quality, respectively (Lintern et al., 2018b; Guo et al., 2019). The aim of this study is to develop an integrated spatio-temporal model using the previously-identified spatial and temporal predictors, and to then assess the performance of this model. Spatio-temporal variability of water quality was modelled using a novel Bayesian hierarchical approach which can jointly account for both variability components, including accounting for varying temporal water quality dynamics between catchments. This modelling approach also has relatively low requirement for input data, which keeps the modelling detail commensurate with the level of data availability. During the model development, we also obtained additional understanding on the patterns of spatial variations in the effects of each temporal predictor. The model can potentially provide useful information for large-scale catchment management, assessment and policy making, such as testing major changes in land use patterns, informing pollution hot-spots, as well as identification and attribution of water quality trends and changes over time.

2. Method

We first discuss the process used to develop the integrated spatio-temporal model (Section 2.1). Sections 2.1.1 and 2.1.2 introduces the statistical modelling framework and the data used for model development, respectively. The approaches to determine model structure was then introduced, which include the choice of key predictors (Section 2.1.3) and the calibration for model parameters (Section 2.1.4). Finally, the approaches to evaluate model performance and robustness are described in Section 2.2.

2.1 Model development

2.1.1 Spatio-temporal modelling framework

A Bayesian hierarchical approach was used to model the spatio-temporal variability in stream water quality. The Bayesian approach enables the inherent natural stochasticity of water quality to be

incorporated into the model (Clark, 2005). A key strength of applying the hierarchical model structure to analyze spatio-temporal variability is that this structure enables the key controls of temporal variability in water quality to vary across locations (Webb and King, 2009;Borsuk et al., 2001). This variability has been found to be important in other study regions where the (temporal) solute export regime varies with catchment characteristics such as climate and land use (Musolff et al., 2015;Poor and McDonnell, 2007).

The structure of the Bayesian hierarchical model is presented below in Eq. 1 to 6. Eq. 1 formulates the transformed constituent concentration (see Section 2.1.2 for justification) at time *i* and site *j* (C_{ij}) as a normally distribution with a mean μ_{ij} and standard deviation σ representing inherent randomness.

$$\boldsymbol{C_{ij} \sim N(\mu_{ij}, \sigma)} \quad (1)$$

To represent spatio-temporal variability, μ_{ij} is modelled as the sum of the site-level mean constituent concentration ($\bar{C}_j$) and the deviation from that mean at time *i* (Δ_{ij}) (Eq. 2).

$$\boldsymbol{\mu_{ij} = \bar{C}_j + \Delta_{ij}} \quad (2)$$

To describe spatial variability, the site-level mean concentration at site *j* ($\bar{C}_j$) is modelled as a linear function of a global intercept (*intC*), and the sum of *m* catchment characteristics $S_{1,j}$ to $S_{m,j}$ (e.g. land use, topography) weighted by their relative contributions to spatial variability (βS_1 to βS_m) (Eq. 3).

$$\boldsymbol{\bar{C}_j = intC + \beta S_1 \times S_{1,j} + \beta S_2 \times S_{2,j} + \cdots + \beta S_m \times S_{m,j}} \quad (3)$$

The temporal variability, represented by the deviation from the mean (Δ_{ij}), is a linear combination of *n* temporal variables, $T_{1,ij}$ to $T_{n,ij}$ (e.g., climate condition, streamflow, vegetation cover) (Eq. 4), at time *i* and site *j*.

$$\boldsymbol{\Delta_{ij} = \beta T_{1,j} \times T_{1,ij} + \cdots + \beta T_{n,j} \times T_{n,ij}} \quad (4)$$

The selection of key spatial and temporal predictors for the model has been performed in our two preceding studies (Lintern et al., 2018b; Guo et al., 2019) and is briefly described in Section 2.1.3. Eq. 1 to 4 enable the model to separately represent the spatial and temporal variability in water quality; however, there is still a further step required to make the model fully spatio-temporal (i.e. being able to predict over both time and location). Specifically, in Guo et al. (2019), clear spatial variation was observed in the relationships between water quality and its key temporal predictors (i.e. in the $\beta T_{N,j}$ in

Eq. 4). To be able to model multiple catchments across a large spatial area simultaneously, we must account for differences in these temporal influences across sites. To do this, the effect of each temporal variable at site *j* ($\beta T_{N,j}$ with *N* in 1,2, … *n*) is drawn from a distribution with a mean of $\mu\beta T_{N,j}$ (Eq. 5), which is then modelled with a linear combination of two additional chatchment characteristics, $ST_{N1,j}$ and $ST_{N2,j}$ (Eq. 6). Details of the selection for these two additional predictors are presented in Section 2.1.3.

$$\boldsymbol{\beta T_{N,j} \sim N(\mu\beta T_{N,j}, \sigma\beta T), for\ N\ in\ 1, 2, \ldots n} \quad (5)$$

$$\boldsymbol{\mu\beta T_{N,j} = intT_N + \beta ST_{N1} \times ST_{N1,j} + \beta ST_{N2} \times ST_{N2,j}} \quad (6)$$

2.1.2 Data collection and processing

The Bayesian hierarchical model was developed with 21 years of monthly stream water quality observations at 102 catchments in the state of Victoria, Australia (aggregate catchment area > 130,000 km^2). The collection and processing of the data are detailed in previous publications that worked with the same dataset (Lintern et al., 2018b; Guo et al., 2019). Briefly, stream water quality data were extracted from the Victorian Water Measurement Information System (Department of Environment Land Water and Planning (DELWP) Victoria, 2016b), which contains monthly grab samples of water quality at approximately 400 sites across Victoria. Water quality data sampled between 1994 and 2014 at 102 sites were used to develop the model (Fig. 1). These sites and time period were chosen because they provided the longest consistent period of continuous records over the greatest number of monitoring sites. The catchments corresponding to these water quality monitoring sites were delineated using the Geofabric tool (Bureau of Meteorology, 2012), and have areas ranging from 5 km^2 to 16,000 km^2. The water quality parameters of interest were: total suspended solids (TSS), total phosphorus (TP), filterable reactive phosphorus (FRP), total Kjeldahl nitrogen (TKN), nitrate-nitrite (NO_x) and electrical conductivity (EC). These parameters represent sediments, nutrients and salts, which are some of the key concerns for water quality managers in Australia and around the world. These water quality samples were collected following standard DELWP protocols (Australian Water Technologies, 1999) and analysed in National Association of Testing Authorities accredited laboratories. Note that in the sampling protocol, FRP is defined as '*Reactive Phosphorus for a filtered sample to a defined filter size (e.g. RP(<0.45 μm))*', which is equivalent to the more widely-used terminology, SRP i.e. Soluble Reactive Phosphorus (Jarvie et al., 2002).

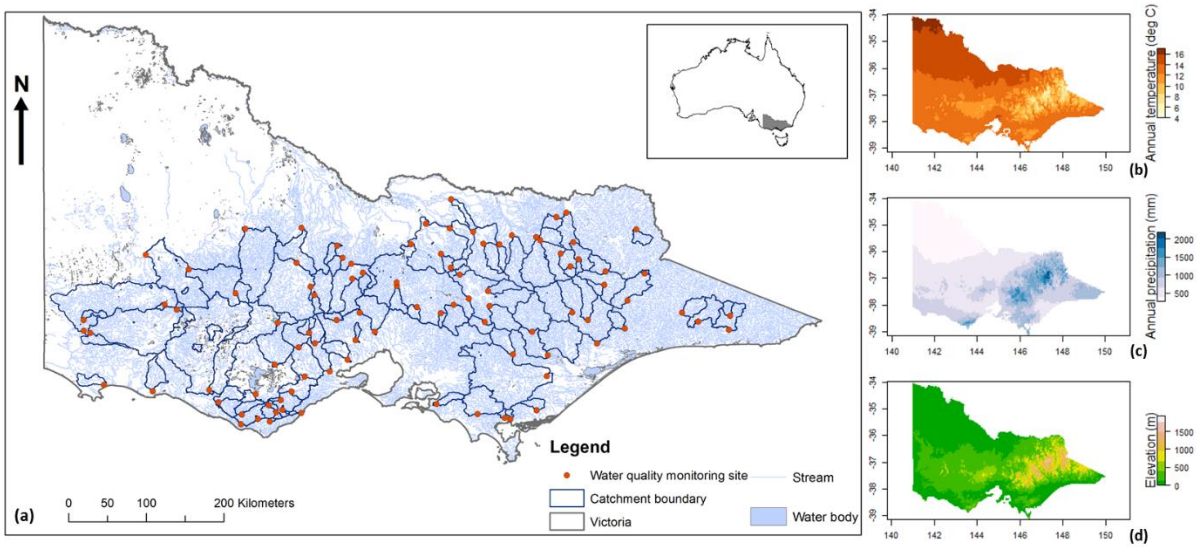

Figure 1. Map of (a) the 102 selected water quality monitoring sites and their catchment boundaries, with inserts showing the location of the state of Victoria within Australia; (b) annual average temperature and (c) annual precipitation and (d) elevation across Victoria.

To compile a dataset for the potential spatial explanatory variables (i.e. predictors to explain spatial variability in water quality), a comprehensive literature review was conducted (Lintern et al., 2018a), which summarized the key catchment landscape characterisitics that are widely known to influence water quality. Further, as part of Lintern et al. (2018b), fifty potential explanatory catchment characteristics were selected, which included catchment land use, land cover, topographic, climatic, geological, lithological and hydrological catchment characteristics. These variables were derived using datasets obtained from Geoscience Australia (2004, 2011), the Bureau of Meteorology (2012), the Bureau of Rural Sciences (2010), Department of Environment Land Water and Planning Victoria (2016) and the Terrestrial Ecosystem Research Network (2016) (see Table S1 in the Supplementary Material for detailed variable names and data sources). We used a static set of land use data from 2005-2006 to represent the entire study period, as a preliminary analysis between 1996 and 2011 suggested less than 1% changes in the key land uses in these catchments (i.e. agricultural, grazing, conservation).

Nineteen potential temporal explanatory variables were included. Firstly, data of discharge (originally in ML d^{-1}) and water temperature (°C) corresponding to the same timestamps for water quality observations were also extracted for each monitoring site over the study period (Department of Environment Land Water and Planning Victoria, 2016). Discharge was converted to runoff depth (mm d^{-1}) for each catchment, and the average streamflows over 1, 3, 7, 14 and 30 days preceding the water quality sampling dates were calculated. In addition, we extracted gridded dataset from the Australian

Water Availability Project (AWAP) (Frost et al., 2016;Raupach et al., 2009, 2012) and Australian Water Resources Assessment Landscape (AWRA-L) model (Frost et al., 2016). These datasets were used to calculate catchment averaged values of daily average temperature (°C), daily rainfall (mm), antecedent rainfall (1, 3, 7, 14 and 30 days preceding sampling), dry spell (> 0.1mm rainfall) length in the antecedent 14 days, daily actual evapotranspiration (ET) (mm), as well as soil moisture for the root-zone and the deep-zone (averaged volumetric content for shallower and deeper than 1m, respectively). In addition, catchment averaged monthly NDVI data were extracted from Advanced Very High Resolution Radiometer (AVHRR) Product (Eidenshink, 1992) and Moderate Resolution Imaging Spectroradiometer MOD13A3 (NASA LP DAAC, 2017). A summary of these datasets of temporal variables and their corresponding sources are in Table S2 in the Supplementary Material and details are provided in Guo et al. 2019.

The raw input data were filtered and transformed to increase the data reliability, continuity and symmetry, making them more suitable for use in the linear spatio-temporal model structure (Eq. 3, 4 and 6). For the filtering process, we first removed all water quality records with flags indicating quality issues. We also removed any values below the detection limit (DL), which was defined as the '*minimum concentration detected for which there is 95% confidence of accuracy and therefore is accurate enough to report*' in the monitoring protocols for this dataset (Australian Water Technologies, 1999). This was because the uncertainty in values below the DL would be amplified after transformation, which would influence the subsequent model fitting. Furthermore, those undetectable low concentrations were of less interest for management purposes. Water quality records corresponding to days with zero flows were also excluded from further analyses.

The transformation process was performed for each of the spatial catchment characteristics, temporal explanatory variables, as well as each water quality constituent to improve the symmetry of individual distributions. The log-sinh transformation (Wang et al., 2012) (Eq. 7) was used for all catchment characteristics, due to its ability to resolve the presence of zero values in several of the catchment characteristics (e.g., percentage area of individual land uses). The *GA* package in R (Luca Scrucca, 2019) was used to identify the log-sinh transformation parameters (a and b) for each spatial explanatory variable that minimized the data skewness (i.e. symmetry is maximized) across all 102 catchments.

$$y_{log-sinh} = \frac{1}{b}\log(\sinh[a + by_{raw}]) \quad (7)$$

In addition, all observed constituent concentrations and temporal explanatory variables were Box-Cox transformed (Box and Cox, 1964) (Eq. 8).

$$y_{Box-Cox} = \begin{cases} \frac{y_{Raw}^{\lambda}-1}{\lambda}, & for\ \lambda \neq 0 \\ logy, & for\ \lambda = 0 \end{cases} \quad (8)$$

For each variable, the optimal Box-Cox transformation parameter λ was identified using the *car* R package and a maximum likelihood-like approach. We first identified the optimal Box-Cox parameter λ using the data at each site (i.e. 21-year time-series). The averaged λ across all sites was then used to transform the data across all catchments together. This transformation approach ensured that all sites used a consistent transformation parameter. All transformation parameters used are summarized in Tables S3 and S4 in the Supplementary Material. The transformation process has greatly improved the data symmetry and thus suitability for use in a linear model (the quality of the transformations was assessed via visual inspection in Lintern et al., 2018b; Guo et al., 2019; and summarized in Figures S2, S4 and S6 in the Supplementary Material).

2.1.3 Selection of key model predictors

Key predictors for the model were selected in a process-informed and data-driven manner based on our two preceding studies (Lintern et al., 2018b; Guo et al., 2019). Lintern et al. (2018b) identified the best spatial predictors (S_1 to S_m in Eq. 3) for the model, while the best temporal predictors across all sites (T_1 to T_n in Eq. 4) have been identified in Guo et al., (2019). In both studies, the best predictors were selected using an exhaustive search approach (May et al., 2011;Saft et al., 2016), which considered all possible combinations of the potential predictors introduced earlier in this section. This selection approach required firstly fitting an individual model to all possible candidate predictor sets, and then comparing all fitted models to select a single best set of predictors. Alternative models were evaluated based on the Akaike Information Criterion (AIC) (Akaike, 1974) and Bayesian Information Criterion (BIC) (Schwarz, 1978) to ensure optimal balance between model performance and complexity.

The best predictors to explain the spatial and temporal variabilities in each constituent are listed in Table 1~~Table 1~~. Generally speaking, the key factors controlling the spatial variability in river water quality were land-use and long-term climate conditions (Lintern et al., 2018b). Temporal variability was mainly

explained by temporal changes in streamflow conditions, water temperature and soil moisture (Guo et al., 2019). The potential mechanisms via which these key drivers influence water quality are discussed in details in these two previous studies.

Table 1. Key factors affecting the spatial and temporal variability for each of six constituents, as identified in Lintern et al. (2018) and Guo et al. (2019b), respectively.

Whilst the previous studies (Lintern et al. 2018b, Guo et al. 2019) identified the predictors for spatial and temporal variability respectively, they did not provide guidance on the predictors for spatial variability in the relationships between drivers of temporal variability and temporal water quality response (i.e. βT in Eq 4). As such, the final step of the predictor selection process to develop the combined spatio-temporal model was to identify the key catchment characteristics that affect spatial variability in the hydroclimatic parameters driving temporal changers in water quality (βT_1 to βT_n in Eq. 4, also right column in Table 1). This is achieved by selecting two spatial characteristics that are most closely related to the coefficient for each temporal predictor (ST_{N1} and ST_{N2}, Eq. 6) across all sites, where only two spatial characteristics were used to avoid over-fitting. Selection of these two spatial characteristics were based on a Spearman correlation analysis between the fitted parameter values of each temporal predictor variable and the fifty potential spatial explanatory variables (as mentioned earlier in this section), following three steps:

1. from the 50 candidate spatial predictors, the one with the highest Spearman correlation with βT_N is selected as ST_{N1}, provided the correlation is statistically significant ($p<0.05$);
2. the subset of remaining spatial predictors with spearman correlation with $ST_{N1} < 0.7$ is found; and
3. from this subset, the spatial predictor with the highest spearman correlation with βT_N is selected as ST_{N2}, provided the correlation has $p<0.05$;

Steps 2 and 3 intended to avoid cross-correlations between ST_{N1} and ST_{N2}. The selected spatial characteristics that influence the temporal relationships in our model are presented and interpreted in Section 3.1. Note that the entire process to select ST_{N1} and ST_{N2} was performed with the fitted parameters for each predictor of the temporal variability obtained from Guo et al. (2019).

2.1.4 Model calibration

After identifying the spatial and temporal predictors for each constituent, as well as the spatial

characteristics which affect the strengths of each temporal predictor, the Bayesian hierarchical spatio-temporal model was fitted for each constituent across all monitoring sites simultaneously. To achieve this, we used the R package *rstan* (Stan Development Team, 2018), which enabled both the sampling of parameter values from posterior distributions with Markov chain Monte Carlo (MCMC) and model evaluation. Constituent standard deviation (σ) was assumed to be drawn from a minimally informative prior half-normal of $N(0,10)$ distribution truncated to only positive values (Gelman, 2006; Stan Development Team, 2018). The regression coefficient of each spatial predictor ($\beta S_1, \beta S_2, \ldots, \beta S_m$ in Eq. 3) was independently drawn from hyper-parameter distributions of $N(\mu\beta S_M, \sigma\beta S_M)$. The site-level regression coefficients of the temporal predictors ($\beta T_{1,j}, \beta T_{2,j}, \ldots, \beta T_{n,j}$ in Eq. 4, respectively) were sampled from the corresponding hyper-parameter distribution of $N(\mu\beta T_N, \sigma\beta T_N)$. The hyper-parameters were further assumed to be drawn from minimally informative prior distributions, following recommendations in Gelman (2006) and Stan Development Team (2019): for all the hyper-parameter means, a normal prior distribution of $N(0,5)$ was used; for all the hyper-parameter standard deviations, a half-normal prior distribution of $N(0,10)$ was used, which was truncated to only positive values. In each model run there were four independent Markov chains. A total of 20,000 iterations were used for each chain. Convergence of the chains was ensured by checking the *Rhat* value (Sturtz et al., 2005), which is a summary statistic on the convergence of the Bayesian models from the four Markov chains used in model calibration (Stan Development Team, 2018). Specifically, an *Rhat* value much greater than 1 indicates that the independent Markov chains have not been mixed well, and a value of below 1.1 is recommended (Stan Development Team, 2018).

2.2 Model performance evaluation and sensitivity analyses

Performance evaluation of the model was undertaken on several aspects of the model results (Section. 3.2). Since the model was calibrated in a Box-Cox transformation scale (see justification in Section 2.1.2), the Box-Cox transformation scale was used for model evaluation to enable a clear investigation on the influences of a wide range of factors that can influence model performance. Detailed performance evaluations include:

1. *Ability to capture total spatio-temporal variability.* Firstly, the simulations from the fitted model and the corresponding observed concentrations were compared at 102 sites altogether to

understand how the overall spatio-temporal variabilities were captured. For each constituent, this evaluation was performed with: 1) these above-DL data to focus only on data used for calibration (as detailed in Section. 2.1.2); and 2) the full dataset including the below-DL data (set to half of the DL of the specific constituent), to understand how well the model represents the full distribution of constituent concentrations. A good model performance when including the below-DL data would suggest that the calibrated model is transferable to below-DL data too. All performance assessments were based on both visual inspection of model fitting as well as the Nash-Sutcliffe efficiency (NSE), which quantified the proportion of variability that was explained by the model (Nash and Sutcliffe, 1970).

2. *Proportions of spatial and temporal variability explained.* This involved a decomposition of the total observed variability using Eq. 2., into proportions contributed by spatial variability (variations in all site-mean concentrations from the grand average of site-mean concentrations) and temporal variability (variations in all concentrations from the corresponding site-mean concentrations). The corresponding modelled values were then used to calculate NSE for each variability component of each constituent.

3. *Ability to capture variation in ambient conditions across space, and temporal variation (including trends) across multiple catchments*. These were evaluated by a) comparing all simulated and observed site-averaged long-term mean concentrations; and b) comparing the simulated and observed time-series and long-term trends at representative sites. Further to a), performance was also evaluated on a real measurement scale by first back-transforming all modelled sample concentrations, calculating the back-transformed site-level means and then compared those to the corresponding observations. A further analysis to b) was also performed by comparing the estimated Sen's slope (Akritas et al., 1995) for the observations and simulations at all sites, and then computing the percentage of sites where the observed trends as indicated by the Sen's slope have been correctly represented by the model.

Additional evaluations of model sensitivity were conducted with calibration and validation on subsets of the full data (Section. 3.3), to understand model transferability and stability:

1. *Model sensitivity to the monitoring sites used for calibration.* We randomly selected 80% of the

sites for calibration and used the remaining 20% for validation, and repeated this validation process 50 times. We compared all calibration and validation performances of these 'partial models' with each other, as well as with the performance of the full model, to obtain a comprehensive evaluation of the sensitivity of model performance to calibration sites.

2. *Model sensitivity to calibration data period.* Since the study region was greatly influenced by a prolonged drought from 1997 to 2009 – known as the Millennium Drought (van Dijk et al., 2013), we also investigated model robustness for before, during and after this drought period. Specifically, we calibrated the model to each pre-, during- and post-drought period (1994-1996, 1997-2009 and 2010-2014, respectively) with model validation on the remaining data. For example, when calibrating to the pre-drought period (1997-2009), validation was performed on the merged during and post-drought period (1994-1996 plus 2010-2014). The corresponding calibration and validation performances were compared with each other as well as against that of the full model, to identify potential impacts of the drought on model robustness.

3. Results

3.1 Spatial variation in the impact of temporal factors

The key controls of the spatial and temporal variations in water quality have been identified in our two preceding studies (Lintern et al. 2018b, Guo et al. 2019) and briefly summarized in Section 2.1.3. and are thus not discussed here. As also detailed in Section 2.1.3, to achieve full spatio-temporal predictive capacity, the model developed in this study considers the spatial variation in the strength of each temporal predictor by using two additional catchment spatial characteristics ($ST_{N1,j}$ and $ST_{N2,j}$ in Eq. 6). on the Spearman's correlations. Here we focus on the most important temporal predictor for each constituent, streamflow, where Table 2 shows the two spatial characteristics identified that are most closely related to the spatial variation of the effects of impact of streamflow on water quality. The full list of the selected key catchment characteristics for all temporal predictors of each constituent is summarized in Table S5 and visualized in Figure S4.

Table 2. The key catchment landscape characteristics that are related to the varying relationships of water quality and same-day streamflow across space, which were selected as the two predictors for the streamflow effect in our model. The corresponding Spearman's correlation (ρ at p<0.05) between the effect of streamflow and each catchment characteristic is presented.

TSS, TP and TKN show consistent patterns of the spatial variation in the effects of streamflow on water

quality, which are strongly driven by the differences in average rainfall conditions across catchments. Specifically, streamflow generally has a larger effect on water quality in catchments with higher average annual rainfall. Since the streamflow effects are positive for the majority of catchments (as shown in Figure S5), these correlations indicate that for the same increase in transformed streamflow, a greater increase in transformed concentrations of TSS, TP and TKN will occur at a catchment with higher annual average rainfall. Given that the Box-Cox lambda values (Table S4) are close to zero, the transformation is log-like and hence changes in transformed flow and concentration approximately correspond to proportional changes in the real values of flow and concentration. In contrast, for FRP, NO_x and EC, the spatial patterns of streamflow effects are specific to each constituent. This difference in the model results between TSS, TP and TKN against the other constituents might be related to the distinct transport pathways of particulate and dissolved constituents. The former is predominantly related to surface flow and thus relies heavily on rainfall contribution. Dissolved constituents are likely transported along the subsurface pathway. Apart from streamflow, the spatial patterns in other key temporal drivers of water quality (e.g. antecedent streamflow, soil moisture etc.) are less consistent across different constituents (Figure S4).

3.2 Model performance evaluation

The spatio-temporal water quality models show varying performances between the constituents. When assessed with only the above-DL data (Fig. 2), the best performing models are those for EC and TKN, which capture 90.7% and 65.8% of the total observed spatio-temporal variability. The modelling performance is lowest for FRP, NO_x and TSS, with NSE values of -1.92, 0.216 and 0.225, respectively. When evaluated against the entire dataset (i.e., including both below- and above DL data), the models explain 19.9% (FRP) to 88.6% (EC) of spatio-temporal variability (Table 3). Model performances for FRP, NO_x and TSS improve notably compared with the previous evaluation of above-DL data, however, they remain as the three constituents that are most difficult to predict. We further discuss the possible factors influencing their model performance in Section 4.1.

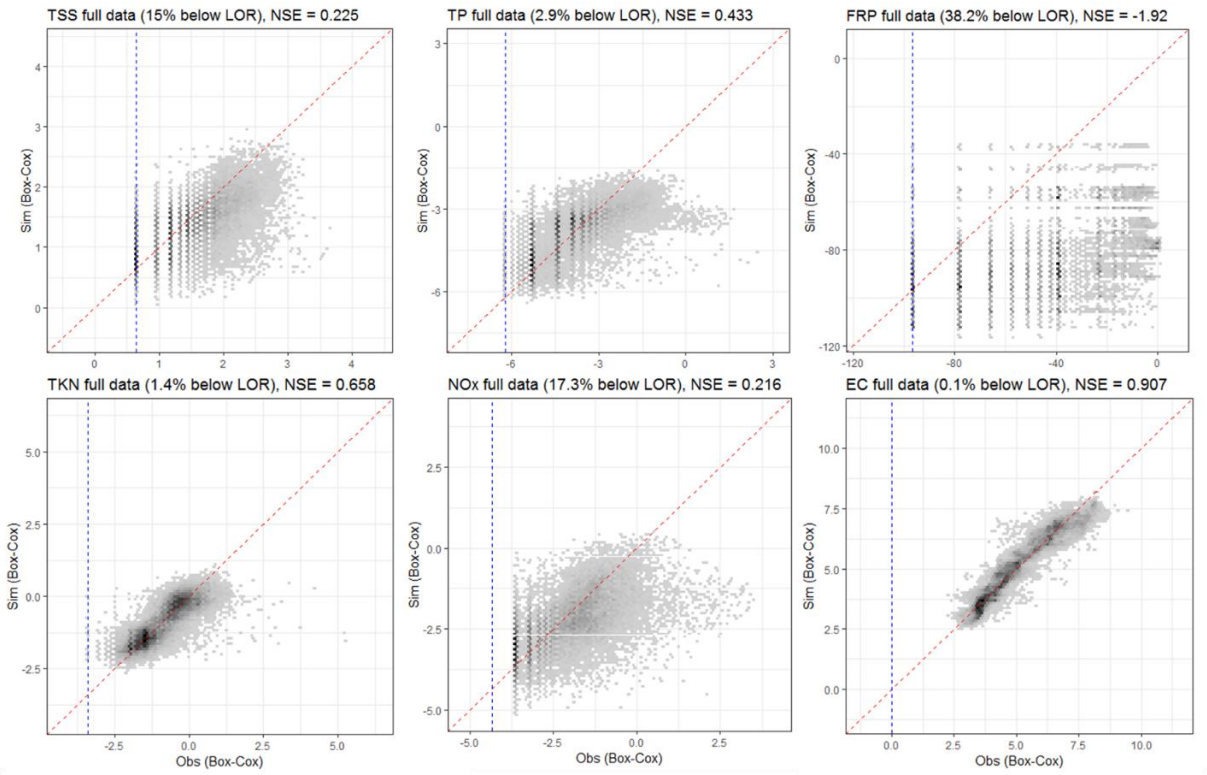

386

387 **Figure 2. Performance of the spatio-temporal models for each of the six constituents,**
388 **represented by the simulated median concentrations and corresponding observations of above-**
389 **DL records across all 102 calibration sites, in Box-Cox transformed space. Darker regions**
390 **represent denser distribution of simulation and observation points. Dashed red lines show the**
391 **1:1 lines whereas dashed blue lines show the DL levels. For each constituent, the percentage of**
392 **data below the DL and the model performance (NSE) are also specified.**

393 **Table 3. Comparison of model performance for all records and only the above-DL~~LOR~~ records**
394 **for each constituent.**

395 The model performance to predict spatial and temporal variability is summarized in Figure 3, which
396 compares the observed and explainable variability for each of the spatial and temporal components
397 (detailed in Section 2.1.4). Regarding the observed variability (lighter colours), EC is strongly
398 dominated by spatial variability (91.8%), highlighting that within-site variation in water quality is
399 minimal compared to between-site variation. To a lesser extent, spatial variability also contributes to
400 major proportions of total variability for TP and TKN (60.8% and 66.6%, respectively). TSS, FRP and
401 NO_x are more influenced by temporal variability (57.4%, 56.6%, 60.5%, respectively).

402

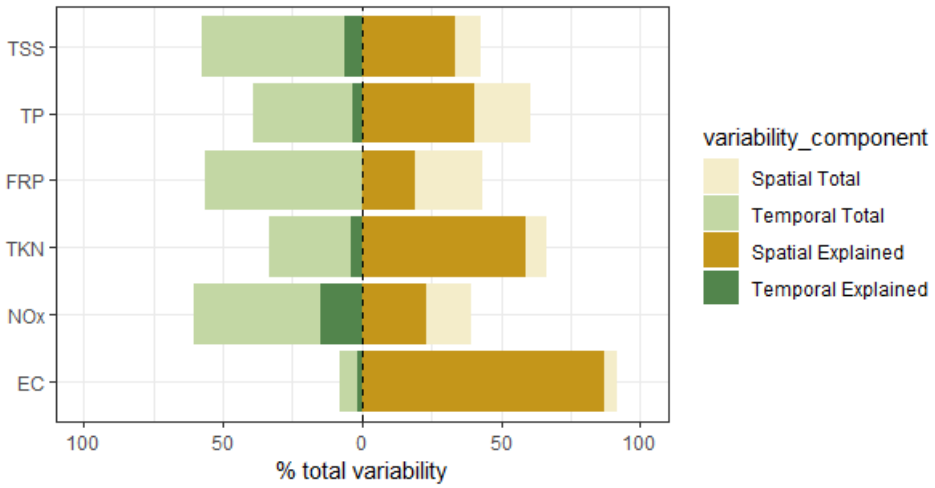

403

404 **Figure 3. Observed spatial and temporal variabilities as proportions of the total variability (total**
405 **width of each bar, 100%). The dashed line differentiates temporal variability (left side) with**
406 **spatial variability (right side), and the darker colours highlight the proportions of spatial and**
407 **temporal variabilities that are explainable by the model. All values were estimated in Box-Cox**
408 **transformed space.**

409 The explained variability (darker colours) show that, across all catchments, temporal variability is much
410 more difficult to model compared with spatial variability. It also appears that a substantial part of the
411 model's overall performance is driven by its ability to capture spatial variability in ambient water quality
412 conditions. For example, the models for TSS, FRP and NO_x show poorer overall performance (Fig. 2,
413 with NSE values of 0.225, -1.92 and 0.216, respectively)), because the total variability for each of these
414 is dominated by temporal variability (57.4%, 56.6%, 60.5%, respectively), which largely remains
415 unexplained by the model (Fig. 3). In contrast, the EC model shows a very good fit with 90.7% of total
416 variability explained – 91.8% of the total observed variability is due to spatial variability, of which
417 94.7% is explained by the model. Therefore, although the EC model can only explain a small portion of
418 temporal variability (20% out of 8.2% of total variability), the overall model performance remains high.

419 As highlighted in Fig. 3, the model has good capacity to capture spatial variability in water quality. This
420 is further evaluated in Fig. 4 by comparing the simulated and observed site-level mean concentrations.
421 The highest model performance is for EC and lowest performance is for FRP (explaining 94.7% and
422 44.2% spatial variability, respectively). At the back-transformed scale, the model shows greater biases
423 for sites with higher concentrations (approximately the highest 10% sites for each constituent) (Fig. 5).
424 This is not surprising as the model was fitted to a Box-Cox transformed space that reduces focus on high
425 values and increases the focused on low values. This compromised its ability to represent sites with

unusually high concentrations. The implications of the model having higher predictive capacity in the transformed scale is further discussed in Section. 4.1.

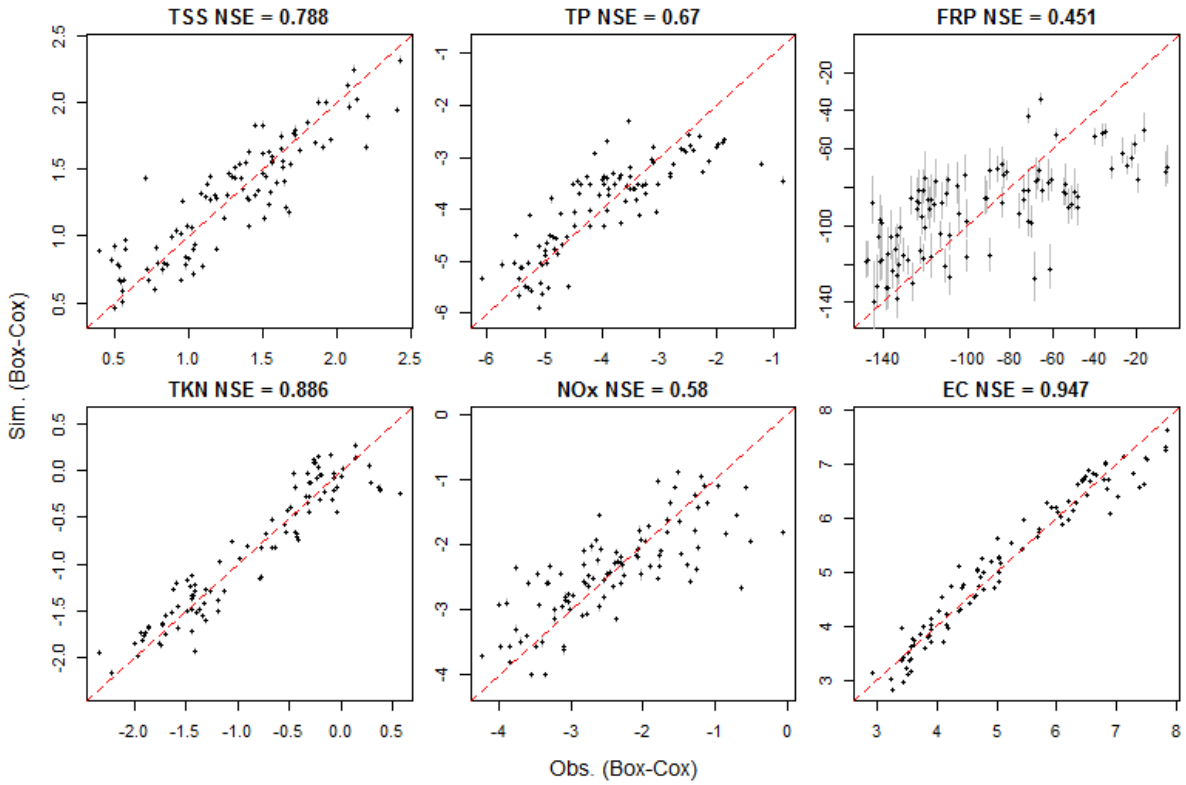

Figure 4. Model fit for site-level mean concentration at the 102 calibration sites for six constituents, with the 95% lower and upper bounds of posterior simulations shown in vertical grey lines. All simulations and observations are presented in in Box-Cox transformed space. The NSE for each constituent is also shown and red dash lines show the 1:1 lines.

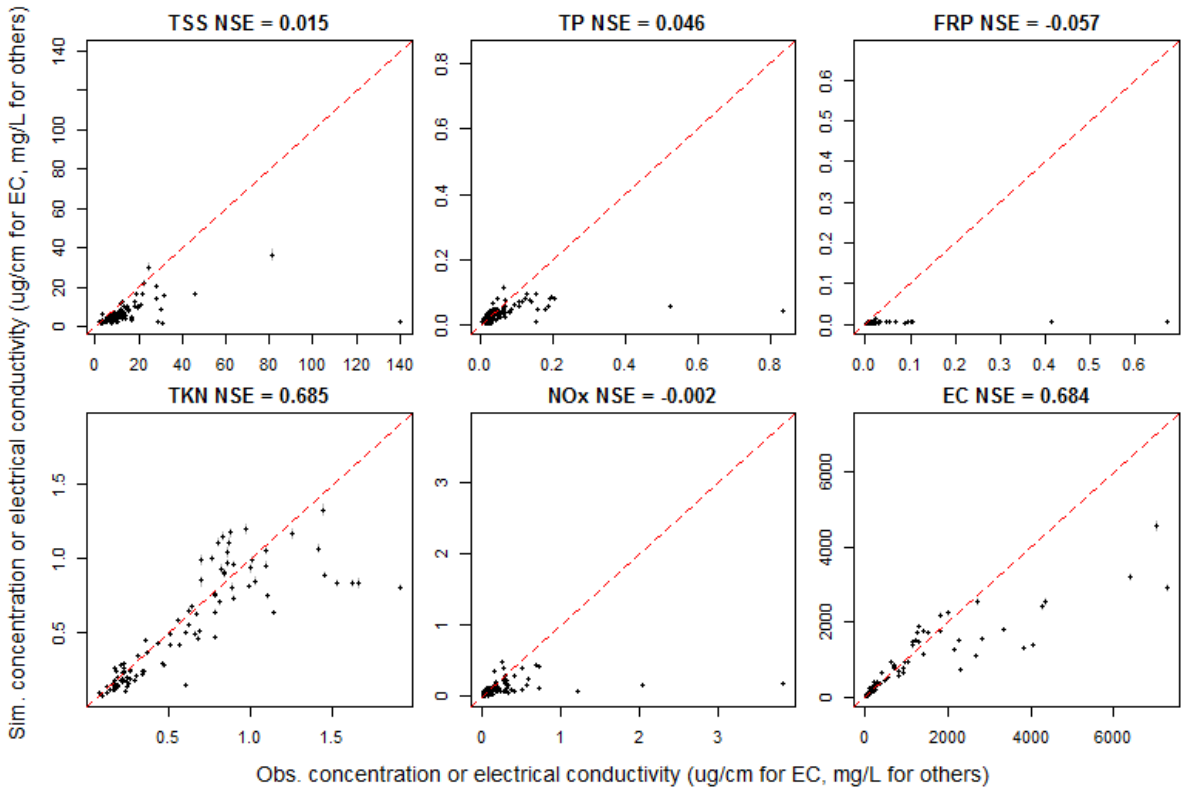

Figure 5. Back-transformation of the model simulations to the measurement scale emphasizes lack of fit for the highest concentrations, illustrated by simulated against observed site-level mean concentrations of each constituent in a back-transformed scale. The 95% lower and upper bounds of all posterior simulations shown in vertical grey lines. The NSE for each constituent is also shown and red dash lines show the 1:1 lines.

As also noted in Fig. 3, the ability of the spatio-temporal model to explain temporal variability remains relatively limited. This is further explored in Fig. 6, where the observed and simulated time-series are presented for one monitoring site for each constituent, at which the model performance (NSE) was the highest. These results show that even for catchments where the model has the highest ability to capture temporal variability, the model consistently underestimated temporal variability for all constituents.

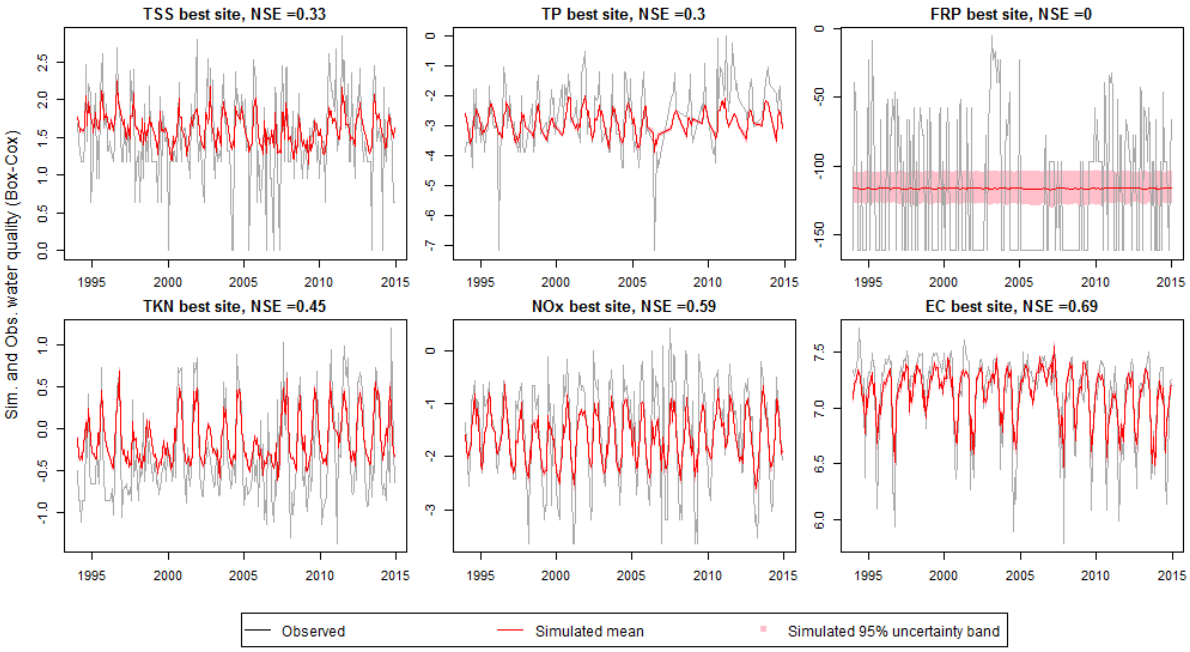

Figure 6. Model fit of the within-site (temporal) water quality variability, illustrated with the observed and simulated time-series for the best-performing site for each constituent. All values are presented in Box-Cox transformed space. The NSE for each constituent is also shown. The red line indicates the corresponding mean of all posterior simulations, while the pink bands show the corresponding 95% lower and upper bounds (only visible for FRP).

Fig. 6 also illustrates that, although the model shows substantial underestimation of temporal variability within site, long-term temporal trends in the time-series are well captured at the best sites (except for FRP). Table 4 summarizes the ability of the model to capture observed trends across all 102 catchments for each constituent. In general, the model is able to capture observed trends in most sites for NO_x and EC and for both positve and negative trends. For TP and TKN, positive trends are well captured while for TSS the negative trends are better captured.

Table 4. Model ability to capture observed water quality trends across all monitoring sites for each constituent. The percentages of sites where observed positive and negative trends are captured by the model are presented separately. Values in brackets indicate numbers of sites where corresponding positive or negative trends are observed. For detailed estimation of these percentages please refer to Sect. 2.2.

3.3 Model sensitivity analyses

We first compare the performance of each spatio-temporal model fitted with the full dataset with those obtained from the 50 corresponding "partial" models that were calibrated to only 80% of the monitoring sites. Note that in this comparison, the FRP model was not assessed due to its poor performance (Section 3.2). The calibration and validation results for the 50 partial models are summarized in Table 5 along

with the performance of the full model calibrated to all 102 sites (see Figs. S6 and S7 in the Supplementary Material for detailed comparison of model residuals of the partial calibration/validation). Across constituents, the calibration performance of the full model was comparable with the 50 partial models. Note the slightly higher calibration performance for the partial models of NO_x compared to the full model. This seems to be related to the generally lower percentages of below-DL data in the 50 randomly-chosen partial calibration datasets (14.1%-17.9%) compared to the full dataset (17.3%) – we further discuss the impacts of below-DL data on model performance in Section 4.1. In addition, model performance is highly consistent between corresponding calibration and validation, with most differences in NSEs less than 0.1. These suggest that the spatio-temporal model performance is highly robust and unaffected by the choice of calibration sites.

Table 5. Comparison of model performances (as NSE) of the full model (Column 2) and the 50 partial models (Columns 3 to 5) with each calibrated to 80% randomly selected monitoring sites. Columns 3 to 5 summarize the mean, minimum and maximum NSE values across the 50 runs, where for each constituent, the top row showing calibration performance and the bottom row showing the validation performance (i.e. at the 20% sites that were not used for calibration).

The performance of the full model for each constituent is also compared with that of the three models calibrated to the pre-, during and post-drought periods. In general, we observe consistent performance for each constituent, across calibrations to the three periods of contrasting hydrological conditions (Table 6, see Figs. S8 to S13 in the Supplementary Material for detailed model fittings). One notable common pattern is that the performance for calibration and validation is more consistent during the drought period than either the pre- and post-drought periods. However, this is most likely explained by relative sizes of the calibration data sets, which are 3, 13 and 5 years for the pre-, during and post-drought periods respectively.

Of all constituents (excluding FRP), TSS shows greater differences in model performances across periods – especially when comparing the pre-drought calibration with its validation for the site-level mean concentrations (Fig. 7). Notably, when calibrated to the pre-drought period and validated on both the during- and post-drought periods, the validated model over-estimates most of the data (Fig. 7 (b));

and when calibrated to the during-drought period, the validated model slightly under-estimates pre- and post-drought period TSS (Fig. 7 (d)).

Table 6. Comparison of model performances (as NSE) of the full model and the three models that were calibrated to the pre-drought (1994-1996), drought (1997-2009) and the post-drought (2010-2014) periods. For each of the models, the calibration performance is shown on the top row and the validation performance (i.e. over the periods that were not used for calibration) is shown on the bottom row. See Section 2.1.4 for details of the calibration and validation approach.

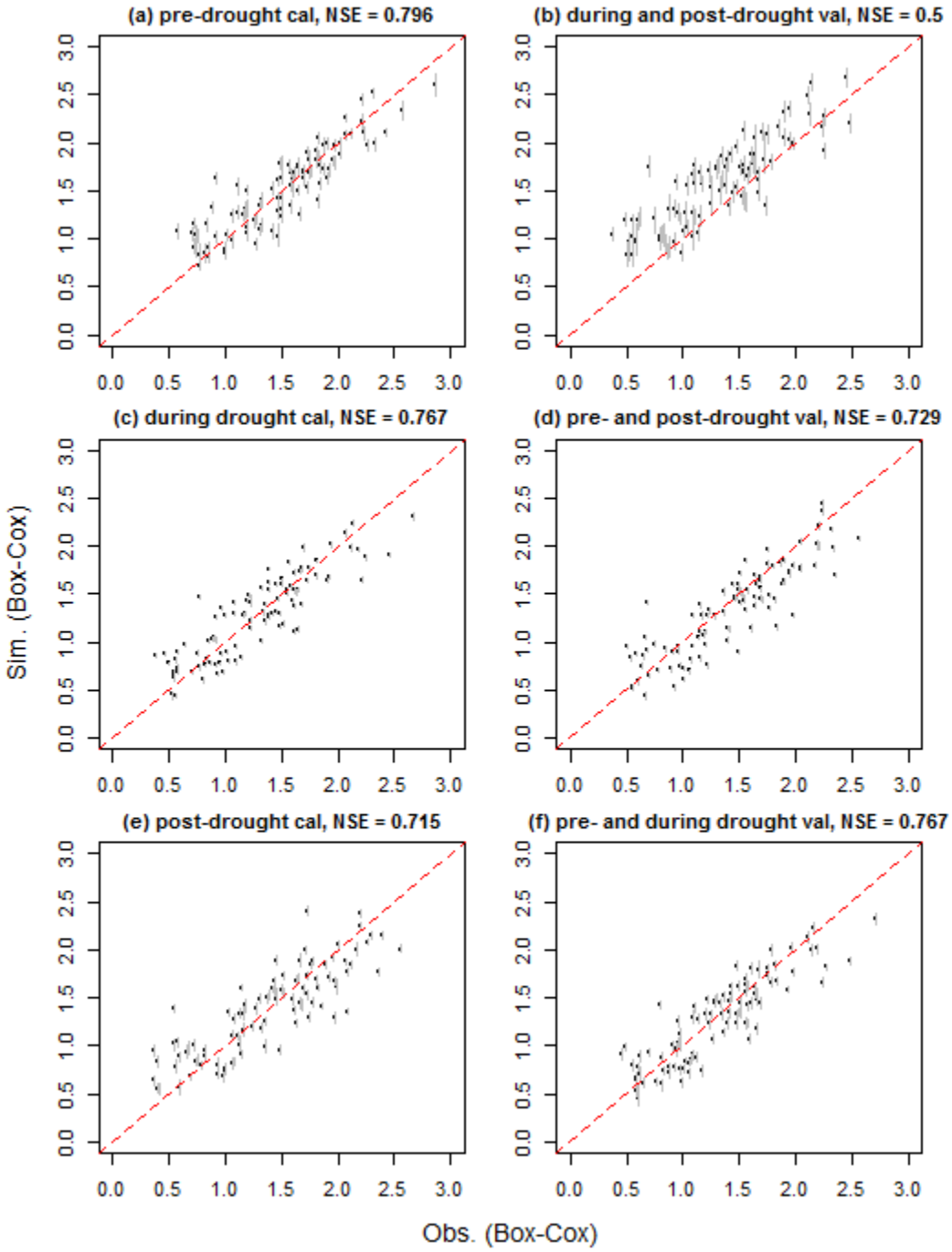

Figure 7. Comparison of the TSS model performance, as the simulated against observed site-level mean concentrations in Box-Cox transformed space. The left column shows calibration performance for the model calibrated to the pre-drought (1994-1996), drought (1997-2009) and the post-drought (2010-2014) periods, respectively; the right column shows the corresponding

validation performance for each period. The 95% lower and upper bounds of simulations shown in vertical grey lines and red dash lines show the 1:1 lines.

The potential impacts of drought on TSS dynamics are further illustrated with the performance of the spatio-temporal model (calibrated to the full dataset with all sites and all data from 1994 to 2014) over the pre-, during and post-drought periods (Fig. 8). Both the during- and post-drought periods have consistently good performances, while the model underestimates most sites for the pre-drought period. This is consistent with Fig. 7 in suggesting a systematic decrease in TSS concentration since the drought began. The better performance of the full model during and after drought (Fig. 8) can be a result of the calibration period of the full spatio-temporal model – between 1994 and 2014 – which was dominated by the during- and post-drought periods.

In summary, Figs 7 and 8 together with Figs. S13-S17 suggest that whilst model performance for most constituents are not affected by the hydrological periods used for calibration and validation, the calibration period did have notable impact on TSS. Some possible causes are discussed in Section 4.3.

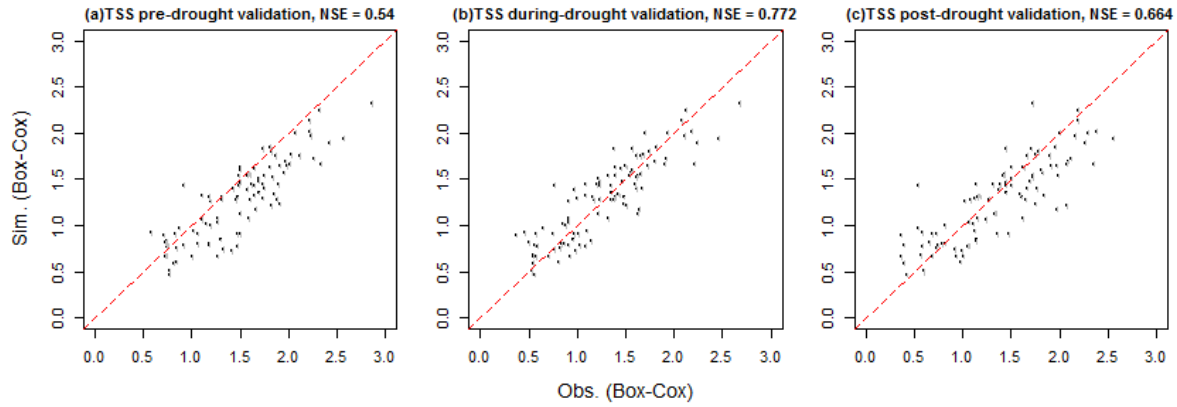

Figure 8. Comparison of the performance of the full spatio-temporal TSS model calibrated to all data across a) pre-drought (1994-1996), b) during drought (1997-2009) and c) post-drought (2010-2014) periods, as represented by the simulated against observed site-level mean concentrations in Box-Cox transformed space. The 95% lower and upper bounds of simulations shown in vertical grey lines and red dash lines show the 1:1 lines.

4. Discussion

4.1 Implications for statistical water quality modelling

In this study, we developed the first process-informed statistical model that is capable of explaining a reasonable proportion of water quality variability for a large spatial area of over 130,000km^2. Although the calibration data have relatively low sampling frequency (i.e. monthly), our model generally performs

satisfactorily in explaining the total variability in water quality. This demonstrates the effectiveness of the Bayesian hierarchical modelling framework in predicting spatio-temporal variability in water quality across large scales. The Bayesian hierarchical model is: a) more advantageous than other simpler statistical water quality models with its more comprehensive and process-informed approach, and capacity to represent varying temporal relationships across large-scale regions; b) less demanding for input data compared with those required by fully-distributed, processes-based models. From a practical perspective, this model has the potential to contribute to a number of management activities including catchment planning, management and policy-making activities, specifically:

1) The spatial predictive capacity can be used to identify pollution hot-spots and the catchment conditions that are likely causes of high concentrations. This can be used to help identify target catchment(s) to prioritize future water quality monitoring and management (Figs. 4 and 5);

2) Further to 1), since water quality has been linked with catchment characteristics in this model, it can also be used to assess potential impacts of alternative options of land use and land cover change, as well as potential effects of climate change, on ambient water quality conditions;

3) The model's temporal predictive capacity can identify changes in water quality due to changes in hydro-climatic conditions and vegetation cover, and thus enabling attribution of detected trends. On the other hand, any 'unexpected' trends can be identified to prompt further investigation to identify causes (Figure 6 and Table 4). The model could also be used for assessing the impacts of long-term catchment changes on water quality (Figures 7 and 8).

Despite the opportunities highlighted above, the model's performance also suggests some current limitations of the modelling framework in the following situations:

~~1)~~ *High within-site temporal variability.* In Section 3.2 we have identified a general lack of predictive power for temporal variability. The potential impacts of high temporal variability on model performance is particularly evident for results of TSS, NO_x and FRP in Fig. 3. Since our model has already included hydro-climatic conditions and vegetation cover to explain temporal variability, the unexplained temporal variability is likely due to other uncaptured temporal drivers. These could be: changes in land use and land management, bio-geochemical processes,

or transit time of water through catchments.

1)

2) *Presence of high proportions of below-DL data.* The full datasets for the three poorly modelled constituents (FRP, TSS and NO_x) all have higher proportions of data below the detection limit (38.2% 17.3% and 15% of all data, respectively) compared with other constituents. As illustrated in Fig. 2, for each of these constituents, removal of below-DL data before model calibration had created clear a truncation on the left-hand side of the distribution. This substantially increases the degrees of skewness and discontinuity of the data, essentially violating the assumption of normally distributed residuals and thus limiting model performance. The model capacity to handle truncated data might be improved by model fitting approaches explicitly designed for this issue. For example, Wang and Robertson (2011) and Zhao et al. (2016) illustrated an approach to resolving the discontinuity of the likelihood estimation in model fitting to data with presence of a lower bound such as zero rainfall values.

3) *Non-conservativeness of constituents.* The results indicate that the reactivity of the constituent is broadly associated with performance, which suggest that bio-geochemical processes (e.g. phosphorus cycling, nitrification/de-nitrification) can make water quality dynamics more difficult for the model to capture. To better capture changes in reactive constituents, the model may require greater consideration of and more extensive spatial and temporal data to represent bio-geochemical processes. Examples include improvements on the process representation for nitrogen cycling and the desorption and adsorption of phosphorus (Granger et al., 2010;Smyth et al., 2013;Tian and Zhou, 2007).

582

583 As previously noted, our model was developed in a Box-Cox transformed scale to ensure the validity of
584 the statistical assumptions (see details on data transformation in Sect. 2.1.2), which shows limited
585 performance for high constituent concentrations when simulations are back-transformed to the
586 measurement scale (Figs. 4 and 5). However, our model approximately represents proportional changes
587 in water quality[1], which can thus help managers to understand proportional changes to inform practical
588 catchment management.

589 For future implementations, the established model structure and parameterization would be best suited

to within the study region. Before performing new simulations (e.g. for new monitoring sites or for current study sites over a different time-period), the statistical properties of the new input datasets should be checked to ensure that they are similar to the calibration datasets. To model new catchments outside of the study region, a re-calibration of the model is required. This would involve extensive selection of key predictors and model calibration, much as performed in this study and the two preceding ones (Lintern et al., 2018b; Guo et al., 2019). A sufficiently long record length (e.g. 20 years) is ideal for such modelling, as it ensures a reasonable understanding of the temporal variability to be obtained.

4.2 Implications for water quality monitoring programs

The current spatio-temporal model extracts water quality temporal variability from monthly data. Utilizing data with higher temporal resolution may further strengthen the model capacity to explain temporal variability, especially by capturing more information on water quality dynamics during flow events. This may be possible into the future; however, current high-frequency water quality sensors (Bende-Michl and Hairsine, 2010;Outram et al., 2014;Lannergård et al., 2019;Pellerin et al., 2016) still have very high resourcing requirements that limits widespread deployment in operational networks.

Furthermore, changes in land use and management over time are currently not considered here as predictors of temporal variability in water quality, which include but not limit to land clearing, urbanization, tillage, fertiliser application and irrigation. This is due to a complete lack, or inconsistency of available data. However, changes in land use/land management practices can occur over short time periods, which can lead to increases in pollutant sources and changes to runoff generation processes (e.g. Tang et al., 2005;DeFries and Eshleman, 2004;Smith et al., 2013). Therefore, our modelling

[1]All Box-Cox transformation parameters for water quality constituents are approximately 0 (Table S4), which means that the transformations are similar to a log transformation.

-framework can potentially be improved by having additional monitoring data on the temporal patterns of land use/land management to better capture their impacts on water quality.

4.3 Potential impacts of long-term drought on water quality dynamics

Results of model calibration and validation to different time periods suggest a systematic decrease in TSS concentrations during and after the prolonged drought, in comparison with the pre-drought period under the same spatial and temporal conditions. Such a shift is not observed for any other five constituents analyzed (nutrients and salts) (Section 3.3).

A further analysis of the calibrated model parameters for pre-, during and post-drought periods suggest that the effects of key spatial predictors do not vary much across periods (Figure S14). In contrast, the effects of key temporal predictors highlight a clear shift in the role of antecedent flow (prior 7-day flow) across different time periods (Figure 9). Specifically, the antecedent flow effects are mostly positive across catchments before the drought, and shift to mostly negative during the drought. After the drought, the antecedent flow effects have mixed directions among different catchments. Considering the limited performance of the TSS model (i.e. substantial under-estimation of temporal variability in Section 3.1), these changing relationships suggested in the calibrated parameters might be unreliable. However, this should not affect the reliability of the observed change in TSS since the drought (Section 3.3), which was based on the systematic differences of model fitting between different periods, revealing a broad-scale patterns across the state on the drought influences.

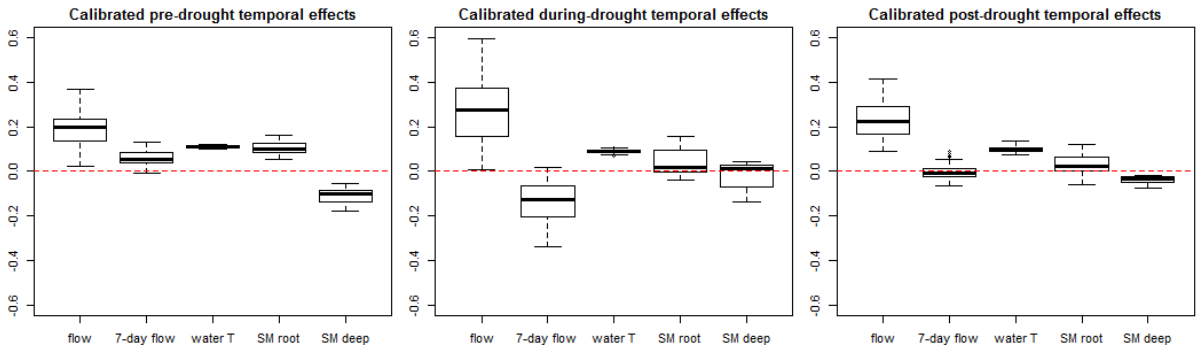

Figure 9. Effects of the five key predictors for the temporal variability in TSS across 102 sites, summarized by the posterior mean of the calibrated parameter values for each predictor (box shows values across all sites), from left: flow, 7-day antecedent flow, water temperature, root-zone soil moisture and deep soil moisture.

In the literature, impacts of the Millennium Drought on the hydrology and runoff regimes of south-eastern Australia are well understood (van Dijk et al., 2013;Leblanc et al., 2012;Saft et al., 2015).

However, less is known about how this major and prolonged drought event has impacted water quality (Bond et al., 2008). Previous studies on other drought events around the world mainly focused on changes in water quality as responses to the reduced streamflow during drought. For example, reduction in sediment levels during drought has been reported and attributed to lower erosion from the contributing catchment, together with lower rates of solid transport associated with reduced flows (Murdoch et al., 2000;Caruso, 2002). At a more local scale, increasing sediment concentrations during drought have also been observed in streams adjacent to land with high densities of livestock and bushland, which both constantly contribute to sediment load during drought, leading to elevated concentrations with lower dilution rate (Caruso, 2002). Similar to sediments, the impact of droughts on stream nutrient and salt concentrations have also commonly been understood as responses to reduced runoff generation and streamflow. In catchments with no significant point-source pollution, nutrient concentrations typically decreased during droughts (Mosley, 2015) with less nutrient leaching and overland flow, but may also increase due to increasing livestock inputs at more local scales (Caruso, 2002). In contrast, catchments with significant point-source pollution generally experience water quality deterioration during drought due to reduced dilution (van Vliet and Zwolsman, 2008;Mosley, 2015). For salinity, concentration often increases during drought with reduced dilution and increased evaporation (Caruso, 2002). This is particularly evident for catchments that are more influenced by saline groundwater input as the relative contribution of groundwater increased during drought (Costelloe et al., 2005).

In contrast to these previous studies, our findings suggest additional possible pathways along which drought can affect stream water quality, that prolonged drought might have altered the relationships between sediments and its predictors (Figs. 7 and 8). In contrast to sediments, our model suggests no clear shifts in the dynamics of nutrients and salts in a regional scale. Our findings are in line with a few previous studies which reported temporal changes in the concentration-discharge relationships for sediments and nutrients, specifically, when comparing high- and low-flow conditions (Zhang, 2018;Moatar et al., 2017), as well as drought and recovery period (Burt et al., 2015). Our findings provide extra dimensions to what would be offered by simple trend analyses using approaches such as Mann Kendall test or Sen's slope (e.g. Smith et al., 1987;Chang, 2008;Hirsch et al., 1991;Bouza-Deaño et al., 2008). Those approaches are only capable of indicating direction and magnitude of observed

663 trends. In contrast, our model was able to attribute the consistent upward shift in TSS concentration to
664 change in relationships between water quality and its key driving factors since the start of drought.

665 In addition, we also acknowledge that our ability to represent the pre- and post-drought conditions in
666 this study may be limited by the record length, since only 2 years of pre-drought and 4 years of post-
667 drought data were available. Once longer records build up, they will enable us to update our
668 understanding of the impact of this prolonged drought. We would be also able to conduct more
669 sophisticated investigations, such as comparing the impacts of long-term droughts versus individual dry
670 and wet years and events (e.g. Saft et al., 2015;Outram et al., 2014;Burt et al., 2015).

671 ## 5. Conclusions

672 This study aims to address the current lack of water quality models that operate at large scales across
673 multiple catchments. To achieve this, we used long-term stream water quality data collected from 102
674 sites in south-eastern Australia, and developed a Bayesian hierarchical statistical model to simulate the
675 spatio-temporal variabilities in six key water quality constituents: TSS, TP, FRP, TKN, NO_x and EC.
676 The choice of model predictors was guided by previous studies on the same dataset (Lintern et al.,
677 2018b; Guo et al., 2019). The model generally well captures the spatio-temporal variability in water
678 quality, where spatial variability between catchments is much better represented than temporal
679 variability. The model is best used to predict proportional changes in water quality in a Box-Cox
680 transformed scale, and can have substantial bias if used to predict absolute values for high
681 concentrations. Cross-validation shows that the spatio-temporal model can predict water quality in non-
682 monitored locations under similar conditions to the historical period and the calibration catchments that
683 we investigated. This can assist management by (1) identifying hot-spots and key temporal periods for
684 waterway pollution; (2) testing effects of catchment changes e.g. urbanization or afforestation; and (3)
685 identifying and attributing major water quality trends and changes.

686 Based on the above model evaluations, we discussed potential ways to further enhance the model
687 performance. In improving the modelling framework, alternative statistical approaches could be
688 considered to reduce the impact of below detection limit data on model performance. In addition, the
689 models could be extended to consider some key bio-geochemical processes to better dynamics in non-
690 conservative constituents (e.g., FRP or NO_x). Regarding data availability, the current models could

potentially benefit from improved monitoring of changes in land use intensity and management to be able to include these drivers in the model. The inclusion of high-frequency water quality sampling data may also extend the model's ability to represent temporal variability. However, high-frequency water quality data are also typically highly variable with large noise. Therefore, the implication of such data for the spatio-temporal modelling framework remains an open question, which needs further investigation in future applications of this modeling framework.

Data availability

All data used in this study were extracted from public domain. All stream water quality data were extracted from the Victorian Water Measurement Information System (via http://data.water.vic.gov.au/, provided by the Department of Environment Land Water and Planning Victoria). The catchments corresponding to these water quality monitoring sites were delineated using the Geofabric tool provided by the Bureau of Meteorology, via ftp://ftp.bom.gov.au/anon/home/geofabric/. We have listed the sources of all other data for the spatial and temporal predictors of our models in Tables S1 and S2 in the Supplementary Materials.

Author contribution

All authors contributed to the conceptualization the models and the design of methodology. A. Lintern and S. Liu contributed to the data curatiom. D.Guo carried out the formal analyses, visualization and validation. J.A. Webb, D. Ryu, U. Bende-Michl and A.W. Western contributed to the funding acquisition. D. Guo, A. Lintern, J.A. Webb, D. Ryu, S. Liu and A.W. Western contributed to the investigation. D. Guo carried out project administration and coding to run the experiments. J.A. Webb, D. Ryu, and A.W. Western contributed to the supervision. D.Guo prepared the manuscript with contributions from all co-authors.

Competing interests

The authors declare that they have no conflict of interest.

Acknowledgement

The Australian Research Council, the Victorian Environment Protection Authority, the Victorian

717 Department of Environment, Land Water and Planning, the Australian Bureau of Meteorology and the
718 Queensland Department of Natural Resources, Mines and Energy provided funding for this project
719 through the linkage program (LP140100495). The authors would also like to thank Matthew Johnson,
720 Louise Sullivan, Hannah Sleeth and Jie Jian, for their assistance in the compilation and analysis of data.
721 All water quality data used for this project can be found on: Water Measurement Information System
722 (http://data.water.vic.gov.au/monitoring.htm). Sources of other data are provided in Tables S1 and S2
723 of the Supplementary Materials.
724

References

Abbaspour, K. C., Rouholahnejad, E., Vaghefi, S., Srinivasan, R., Yang, H., and Kløve, B.: A continental-scale hydrology and water quality model for Europe: Calibration and uncertainty of a high-resolution large-scale SWAT model, Journal of Hydrology, 524, 733-752, https://doi.org/10.1016/j.jhydrol.2015.03.027, 2015.

Adams, R., Arafat, Y., Eate, V., Grace, M. R., Saffarpour, S., Weatherley, A. J., and Western, A. W.: A catchment study of sources and sinks of nutrients and sediments in south-east Australia, Journal of Hydrology, 515, 166-179, https://doi.org/10.1016/j.jhydrol.2014.04.034, 2014.

Ahearn, D. S., Sheibley, R. W., Dahlgren, R. A., and Keller, K. E.: Temporal dynamics of stream water chemistry in the last free-flowing river draining the western Sierra Nevada, California, Journal of Hydrology, 295, 47-63, https://doi.org/10.1016/j.jhydrol.2004.02.016, 2004.

Ai, L., Shi, Z. H., Yin, W., and Huang, X.: Spatial and seasonal patterns in stream water contamination across mountainous watersheds: Linkage with landscape characteristics, Journal of Hydrology, 523, 398-408, https://doi.org/10.1016/j.jhydrol.2015.01.082, 2015.

Akaike, H.: A new look at the statistical model identification, IEEE transactions on automatic control, 19, 716-723, 1974.

Akritas, M. G., Murphy, S. A., and Lavalley, M. P.: The Theil-Sen estimator with doubly censored data and applications to astronomy, Journal of the American Statistical Association, 90, 170-177, 1995.

Ali, G., Wilson, H., Elliott, J., Penner, A., Haque, A., Ross, C., and Rabie, M.: Phosphorus export dynamics and hydrobiogeochemical controls across gradients of scale, topography and human impact, Hydrological Processes, 31, 3130-3145, 10.1002/hyp.11258, 2017.

Australian Water Technologies: Victorian water quality monitoring network and state biological monitoring programme manual of procedures, Australian Water Technologies, 68 Ricketts Rd, Mt Waverley VIC 3149, 1999.

Bailey, R. T., and Ahmadi, M.: Spatial and temporal variability of in-stream water quality parameter influence on dissolved oxygen and nitrate within a regional stream network, Ecological modelling, 277, 87-96, 2014.

Bende-Michl, U., and Hairsine, P. B.: A systematic approach to choosing an automated nutrient analyser for river monitoring, Journal of Environmental Monitoring, 12, 127-134, 2010.

Bond, N. R., Lake, P. S., and Arthington, A. H.: The impacts of drought on freshwater ecosystems: an Australian perspective, Hydrobiologia, 600, 3-16, 10.1007/s10750-008-9326-z, 2008.

Borsuk, M. E., Higdon, D., Stow, C. A., and Reckhow, K. H.: A Bayesian hierarchical model to predict benthic oxygen demand from organic matter loading in estuaries and coastal zones, Ecological Modelling, 143, 165-181, https://doi.org/10.1016/S0304-3800(01)00328-3, 2001.

Bouza-Deaño, R., Ternero-Rodríguez, M., and Fernández-Espinosa, A. J.: Trend study and assessment of surface water quality in the Ebro River (Spain), Journal of Hydrology, 361, 227-239, https://doi.org/10.1016/j.jhydrol.2008.07.048, 2008.

Box, G. E., and Cox, D. R.: An analysis of transformations, Journal of the Royal Statistical Society: Series B (Methodological), 26, 211-243, 1964.

Bureau of Meteorology: Geofabric V2 2012.

Bureau of Rural Sciences: 2005/06 Land use of Australia, version 4. . 2010.

Burt, T. P., Worrall, F., Howden, N. J. K., and Anderson, M. G.: Shifts in discharge-concentration relationships as a small catchment recover from severe drought, Hydrological Processes, 29, 498-507, 10.1002/hyp.10169, 2015.

Carey, R. O., and Migliaccio, K. W.: Contribution of wastewater treatment plant effluents to nutrient dynamics in aquatic systems: a review, Environ Manage, 44, 205-217, 10.1007/s00267-009-9309-5, 2009.

Caruso, B. S.: Temporal and spatial patterns of extreme low flows and effects on stream ecosystems in Otago, New Zealand, Journal of Hydrology, 257, 115-133, https://doi.org/10.1016/S0022-1694(01)00546-7, 2002.

Chang, H.: Spatial analysis of water quality trends in the Han River basin, South Korea, Water Research, 42, 3285-3304, https://doi.org/10.1016/j.watres.2008.04.006, 2008.

Clark, J. S.: Why environmental scientists are becoming Bayesians, Ecology Letters, 8, 2-14, doi:10.1111/j.1461-0248.2004.00702.x, 2005.
Costelloe, J. F., Grayson, R. B., McMahon, T. A., and Argent, R. M.: Spatial and temporal variability of water salinity in an ephemeral, arid-zone river, central Australia, Hydrological Processes, 19, 3147-3166, 10.1002/hyp.5837, 2005.
DeFries, R., and Eshleman, K. N.: Land-use change and hydrologic processes: a major focus for the future, Hydrological Processes, 18, 2183-2186, doi:10.1002/hyp.5584, 2004.
Department of Environment Land Water and Planning Victoria: Victorian water measurement information system. . 2016.
Eidenshink, J. C.: The 1990 Conterminous U.S. AVHRR Data Set, Photogrammetric Engineering and Remote Sensing, 58, 1992.
Fraser, A. I., Harrod, T. R., and Haygarth, P. M.: The effect of rainfall intensity on soil erosion and particulate phosphorus transfer from arable soils, Water Science and Technology, 39, 41-45, https://doi.org/10.1016/S0273-1223(99)00316-9, 1999.
Frost, A. J., Ramchurn, A., and Smith, A.: The bureau's operational AWRA landscape (AWRA-L) Model, Bureau of Meteorology, 2016.
Fu, B., Merritt, W. S., Croke, B. F. W., Weber, T., and Jakeman, A. J.: A review of catchment-scale water quality and erosion models and a synthesis of future prospects, Environmental Modelling & Software, https://doi.org/10.1016/j.envsoft.2018.12.008, 2018.
Gelman, A.: Prior distributions for variance parameters in hierarchical models (comment on article by Browne and Draper), Bayesian Anal., 1, 515-534, 10.1214/06-BA117A, 2006.
Geoscience Australia: Dams and water storages. . 2004.
Geoscience Australia: Environmental Attributes Dataset. 2011.
Giri, S., and Qiu, Z.: Understanding the relationship of land uses and water quality in Twenty First Century: A review, Journal of Environmental Management, 173, 41-48, https://doi.org/10.1016/j.jenvman.2016.02.029, 2016.
Granger, S. J., Bol, R., Anthony, S., Owens, P. N., White, S. M., and Haygarth, P. M.: Chapter 3 - Towards a Holistic Classification of Diffuse Agricultural Water Pollution from Intensively Managed Grasslands on Heavy Soils, in: Advances in Agronomy, Academic Press, 83-115, 2010.
Guo, D., Lintern, A., Webb, J. A., Ryu, D., Liu, S., Bende-Michl, U., Leahy, P., Wilson, P., and Western, A. W.: Key Factors Affecting Temporal Variability in Stream Water Quality, Water Resources Research, 55, 112-129, 10.1029/2018wr023370, 2019.
Heathwaite, A. L.: Multiple stressors on water availability at global to catchment scales: understanding human impact on nutrient cycles to protect water quality and water availability in the long term, Freshwater Biology, 55, 241-257, 10.1111/j.1365-2427.2009.02368.x, 2010.
Hirsch, R. M., Alexander, R. B., and Smith, R. A.: Selection of methods for the detection and estimation of trends in water quality, Water Resources Research, 27, 803-813, 10.1029/91wr00259, 1991.
Hrachowitz, M., Benettin, P., van Breukelen, B. M., Fovet, O., Howden, N. J. K., Ruiz, L., van der Velde, Y., and Wade, A. J.: Transit times—the link between hydrology and water quality at the catchment scale, Wiley Interdisciplinary Reviews: Water, 3, 629-657, doi:10.1002/wat2.1155, 2016.
Jarvie, H. P., Withers, J., and Neal, C.: Review of robust measurement of phosphorus in river water: sampling, storage, fractionation and sensitivity, Hydrology and Earth System Sciences, 6, 113-131, 2002.
Kingsford, R. T., Walker, K. F., Lester, R. E., Young, W. J., Fairweather, P. G., Sammut, J., and Geddes, M. C.: A Ramsar wetland in crisis – the Coorong, Lower Lakes and Murray Mouth, Australia, Marine and Freshwater Research, 62, 255-265, https://doi.org/10.1071/MF09315, 2011.
Kisi, O., and Parmar, K. S.: Application of least square support vector machine and multivariate adaptive regression spline models in long term prediction of river water pollution, Journal of Hydrology, 534, 104-112, https://doi.org/10.1016/j.jhydrol.2015.12.014, 2016.
Kurunç, A., Yürekli, K., and Çevik, O.: Performance of two stochastic approaches for forecasting water quality and streamflow data from Yeşilırmak River, Turkey, Environmental Modelling & Software, 20, 1195-1200, https://doi.org/10.1016/j.envsoft.2004.11.001, 2005.

Lannergård, E. E., Ledesma, J. L., Fölster, J., and Futter, M. N.: An evaluation of high frequency turbidity as a proxy for riverine total phosphorus concentrations, Science of the Total Environment, 651, 103-113, 2019.
Leblanc, M., Tweed, S., Van Dijk, A., and Timbal, B.: A review of historic and future hydrological changes in the Murray-Darling Basin, Global and Planetary Change, 80-81, 226-246, https://doi.org/10.1016/j.gloplacha.2011.10.012, 2012.
Lintern, A., Webb, J. A., Ryu, D., Liu, S., Bende-Michl, U., Waters, D., Leahy, P., Wilson, P., and Western, A. W.: Key factors influencing differences in stream water quality across space, Wiley Interdisciplinary Reviews: Water, 5, e1260, doi:10.1002/wat2.1260, 2018a.
Lintern, A., Webb, J. A., Ryu, D., Liu, S., Waters, D., Leahy, P., Bende-Michl, U., and Western, A. W.: What Are the Key Catchment Characteristics Affecting Spatial Differences in Riverine Water Quality?, Water Resources Research, doi:10.1029/2017WR022172, 2018b.
Luca Scrucca: Package 'GA', The Comprehensive R Archive Network,, 2019.
May, R., Dandy, G., and Maier, H.: Review of input variable selection methods for artificial neural networks, in: Artificial neural networks-methodological advances and biomedical applications, InTech, 2011.
Mellander, P.-E., Jordan, P., Shore, M., Melland, A. R., and Shortle, G.: Flow paths and phosphorus transfer pathways in two agricultural streams with contrasting flow controls, Hydrological Processes, 29, 3504-3518, doi:10.1002/hyp.10415, 2015.
Meybeck, M., and Helmer, R.: The quality of rivers: From pristine stage to global pollution, Palaeogeography, Palaeoclimatology, Palaeoecology, 75, 283-309, https://doi.org/10.1016/0031-0182(89)90191-0, 1989.
Miller, C., Magdalina, A., Willows, R. I., Bowman, A. W., Scott, E. M., Lee, D., Burgess, C., Pope, L., Pannullo, F., and Haggarty, R.: Spatiotemporal statistical modelling of long-term change in river nutrient concentrations in England & Wales, Science of The Total Environment, 466-467, 914-923, https://doi.org/10.1016/j.scitotenv.2013.07.113, 2014.
Moatar, F., Abbott, B. W., Minaudo, C., Curie, F., and Pinay, G.: Elemental properties, hydrology, and biology interact to shape concentration-discharge curves for carbon, nutrients, sediment, and major ions, Water Resources Research, 53, 1270-1287, 10.1002/2016wr019635, 2017.
Mosley, L. M.: Drought impacts on the water quality of freshwater systems; review and integration, Earth-Science Reviews, 140, 203-214, https://doi.org/10.1016/j.earscirev.2014.11.010, 2015.
Murdoch, P. S., Baron, J. S., and Miller, T. L.: POTENTIAL EFFECTS OF CLIMATE CHANGE ON SURFACE-WATER QUALITY IN NORTH AMERICA1, JAWRA Journal of the American Water Resources Association, 36, 347-366, 10.1111/j.1752-1688.2000.tb04273.x, 2000.
Musolff, A., Schmidt, C., Selle, B., and Fleckenstein, J. H.: Catchment controls on solute export, Advances in Water Resources, 86, 133-146, https://doi.org/10.1016/j.advwatres.2015.09.026, 2015.
NASA LP DAAC: MOD13A3: MODIS/Terra Vegetation Indices Monthly L3 Global 1km V005. 2017.
Onderka, M., Wrede, S., Rodný, M., Pfister, L., Hoffmann, L., and Krein, A.: Hydrogeologic and landscape controls of dissolved inorganic nitrogen (DIN) and dissolved silica (DSi) fluxes in heterogeneous catchments, Journal of Hydrology, 450-451, 36-47, https://doi.org/10.1016/j.jhydrol.2012.05.035, 2012.
Outram, F. N., Lloyd, C. E. M., Jonczyk, J., Benskin, C. M. H., Grant, F., Perks, M. T., Deasy, C., Burke, S. P., Collins, A. L., Freer, J., Haygarth, P. M., Hiscock, K. M., Johnes, P. J., and Lovett, A. L.: High-frequency monitoring of nitrogen and phosphorus response in three rural catchments to the end of the 2011–2012 drought in England, Hydrol. Earth Syst. Sci., 18, 3429-3448, 10.5194/hess-18-3429-2014, 2014.
Ouyang, W., Hao, F., Skidmore, A. K., and Toxopeus, A. G.: Soil erosion and sediment yield and their relationships with vegetation cover in upper stream of the Yellow River, Science of The Total Environment, 409, 396-403, https://doi.org/10.1016/j.scitotenv.2010.10.020, 2010.
Parmar, K. S., and Bhardwaj, R.: Statistical, time series, and fractal analysis of full stretch of river Yamuna (India) for water quality management, Environmental Science and Pollution Research, 22, 397-414, 10.1007/s11356-014-3346-1, 2015.
Pellerin, B. A., Stauffer, B. A., Young, D. A., Sullivan, D. J., Bricker, S. B., Walbridge, M. R., Clyde Jr., G. A., and Shaw, D. M.: Emerging Tools for Continuous Nutrient Monitoring Networks: Sensors Advancing

881 Science and Water Resources Protection, JAWRA Journal of the American Water Resources Association,
882 52, 993-1008, 10.1111/1752-1688.12386, 2016.
883 Poor, C. J., and McDonnell, J. J.: The effects of land use on stream nitrate dynamics, Journal of
884 Hydrology, 332, 54-68, https://doi.org/10.1016/j.jhydrol.2006.06.022, 2007.
885 Poudel, D. D., Lee, T., Srinivasan, R., Abbaspour, K., and Jeong, C. Y.: Assessment of seasonal and spatial
886 variation of surface water quality, identification of factors associated with water quality variability, and
887 the modeling of critical nonpoint source pollution areas in an agricultural watershed, Journal of Soil
888 and Water Conservation, 68, 155-171, 10.2489/jswc.68.3.155, 2013.
889 Poulsen, D. L., Simmons, C. T., Le Galle La Salle, C., and Cox, J. W.: Assessing catchment-scale spatial
890 and temporal patterns of groundwater and stream salinity, Hydrogeology Journal, 14, 1339-1359,
891 10.1007/s10040-006-0065-9, 2006.
892 Qin, B., Zhu, G., Gao, G., Zhang, Y., Li, W., Paerl, H. W., and Carmichael, W. W.: A Drinking Water Crisis
893 in Lake Taihu, China: Linkage to Climatic Variability and Lake Management, Environmental
894 Management, 45, 105-112, 10.1007/s00267-009-9393-6, 2010.
895 Raupach, M., Briggs, P., Haverd, V., King, E., Paget, M., and Trudinger, C.: Australian water availability
896 project (AWAP): CSIRO marine and atmospheric research component: final report for phase 3, 67, 2009.
897 Raupach, M., Briggs, P., Haverd, V., King, E., Paget, M., and Trudinger, C.: Australian Water Availability
898 Project. CSIRO Marine and Atmospheric Research, Canberra, Australia., 2012.
899 Ren, W., Zhong, Y., Meligrana, J., Anderson, B., Watt, W. E., Chen, J., and Leung, H.-L.: Urbanization,
900 land use, and water quality in Shanghai: 1947–1996, Environment International, 29, 649-659,
901 https://doi.org/10.1016/S0160-4120(03)00051-5, 2003.
902 Saft, M., Western, A. W., Zhang, L., Peel, M. C., and Potter, N. J.: The influence of multiyear drought on
903 the annual rainfall-runoff relationship: An Australian perspective, Water Resources Research, 51, 2444-
904 2463, doi:10.1002/2014WR015348, 2015.
905 Saft, M., Peel, M. C., Western, A. W., and Zhang, L.: Predicting shifts in rainfall-runoff partitioning
906 during multiyear drought: Roles of dry period and catchment characteristics, Water Resources
907 Research, 52, 9290-9305, doi:10.1002/2016WR019525, 2016.
908 Schwarz, G.: Estimating the dimension of a model, The annals of statistics, 6, 461-464, 1978.
909 Sharpley, A. N., Kleinman, P. J. A., McDowell, R. W., Gitau, M., and Bryant, R. B.: Modeling phosphorus
910 transport in agricultural watersheds: Processes and possibilities, Journal of Soil and Water
911 Conservation, 57, 425-439, 2002.
912 Smith, A. P., Western, A. W., and Hannah, M. C.: Linking water quality trends with land use
913 intensification in dairy farming catchments, Journal of Hydrology, 476, 1-12, 2013.
914 Smith, R. A., Alexander, R. B., and Wolman, M. G.: Water-Quality Trends in the Nation's Rivers, Science,
915 235, 1607-1615, 1987.
916 Smyth, A. R., Thompson, S. P., Siporin, K. N., Gardner, W. S., McCarthy, M. J., and Piehler, M. F.:
917 Assessing nitrogen dynamics throughout the estuarine landscape, Estuaries and coasts, 36, 44-55, 2013.
918 Stan Development Team: RStan: the R interface to Stan. R package version 2.18.1, 2018.
919 Stan Reference Manual Version 2.20: https://mc-stan.org/docs/2_20/reference-manual-2_20.pdf,
920 access: 28/09/2019, 2019.
921 Sueker, J. K., Clow, D. W., Ryan, J. N., and Jarrett, R. D.: Effect of basin physical characteristics on solute
922 fluxes in nine alpine/subalpine basins, Colorado, USA, Hydrological Processes, 15, 2749-2769,
923 10.1002/hyp.265, 2001.
924 Tang, Z., Engel, B. A., Pijanowski, B. C., and Lim, K. J.: Forecasting land use change and its environmental
925 impact at a watershed scale, Journal of Environmental Management, 76, 35-45,
926 https://doi.org/10.1016/j.jenvman.2005.01.006, 2005.
927 Terrestrial Ecosystem Research Network: Soil and landscape grid of Australia. 2016.
928 Tian, J. R., and Zhou, P. J.: Phosphorus fractions of floodplain sediments and phosphorus exchange on
929 the sediment–water interface in the lower reaches of the Han River in China, Ecological Engineering,
930 30, 264-270, https://doi.org/10.1016/j.ecoleng.2007.01.006, 2007.
931 Tramblay, Y., Ouarda, T. B. M. J., St-Hilaire, A., and Poulin, J.: Regional estimation of extreme suspended
932 sediment concentrations using watershed characteristics, Journal of Hydrology, 380, 305-317,
933 https://doi.org/10.1016/j.jhydrol.2009.11.006, 2010.

van Dijk, A. I. J. M., Beck, H. E., Crosbie, R. S., de Jeu, R. A. M., Liu, Y. Y., Podger, G. M., Timbal, B., and Viney, N. R.: The Millennium Drought in southeast Australia (2001–2009): Natural and human causes and implications for water resources, ecosystems, economy, and society, Water Resources Research, 49, 1040-1057, 10.1002/wrcr.20123, 2013.
van Vliet, M. T. H., and Zwolsman, J. J. G.: Impact of summer droughts on the water quality of the Meuse river, Journal of Hydrology, 353, 1-17, https://doi.org/10.1016/j.jhydrol.2008.01.001, 2008.
Varanka, S., Hjort, J., and Luoto, M.: Geomorphological factors predict water quality in boreal rivers, Earth Surface Processes and Landforms, 40, 1989-1999, 10.1002/esp.3601, 2015.
Vörösmarty, C. J., McIntyre, P. B., Gessner, M. O., Dudgeon, D., Prusevich, A., Green, P., Glidden, S., Bunn, S. E., Sullivan, C. A., Liermann, C. R., and Davies, P. M.: Global threats to human water security and river biodiversity, Nature, 467, 555, 10.1038/nature09440

https://www.nature.com/articles/nature09440#supplementary-information, 2010.
Wang, Q. J., and Robertson, D. E.: Multisite probabilistic forecasting of seasonal flows for streams with zero value occurrences, Water Resources Research, 47, 10.1029/2010wr009333, 2011.
Wang, Q. J., Shrestha, D. L., Robertson, D. E., and Pokhrel, P.: A log-sinh transformation for data normalization and variance stabilization, Water Resources Research, 48, doi:10.1029/2011WR010973, 2012.
Webb, J. A., and King, L. E.: A Bayesian hierarchical trend analysis finds strong evidence for large-scale temporal declines in stream ecological condition around Melbourne, Australia, Ecography, 32, 215-225, doi:10.1111/j.1600-0587.2008.05686.x, 2009.
Whitworth, K. L., Baldwin, D. S., and Kerr, J. L.: Drought, floods and water quality: Drivers of a severe hypoxic blackwater event in a major river system (the southern Murray–Darling Basin, Australia), Journal of Hydrology, 450-451, 190-198, https://doi.org/10.1016/j.jhydrol.2012.04.057, 2012.
Zhang, Q., and Ball, W. P.: Improving riverine constituent concentration and flux estimation by accounting for antecedent discharge conditions, Journal of Hydrology, 547, 387-402, https://doi.org/10.1016/j.jhydrol.2016.12.052, 2017.
Zhang, Q.: Synthesis of nutrient and sediment export patterns in the Chesapeake Bay watershed: Complex and non-stationary concentration-discharge relationships, Science of The Total Environment, 618, 1268-1283, https://doi.org/10.1016/j.scitotenv.2017.09.221, 2018.
Zhao, T., Schepen, A., and Wang, Q. J.: Ensemble forecasting of sub-seasonal to seasonal streamflow by a Bayesian joint probability modelling approach, Journal of Hydrology, 541, 839-849, https://doi.org/10.1016/j.jhydrol.2016.07.040, 2016.
Zhou, T., Wu, J., and Peng, S.: Assessing the effects of landscape pattern on river water quality at multiple scales: A case study of the Dongjiang River watershed, China, Ecological Indicators, 23, 166-175, https://doi.org/10.1016/j.ecolind.2012.03.013, 2012.

Tables

Table 1. Key factors affecting the spatial and temporal variability for each of six constituents, as identified in Lintern et al. (2018) and Guo et al. (2019b), respectively.

Constituent	Key factors that affect spatial variability	Key factors that affect
TSS	Hottest month maximum temperature	Same-day streamflow
	Percentage area covered by grass	7-day antecedent streamflow
	Percentage area covered by shrub	Water temperature
	Percentage cropping area	Soil moisture root
	Maximum elevation	Soil moisture deep
	Dam storage	
	Percentage clay area	
TP	Erosivity	Same-day streamflow
	Percentage area covered by grass	30-day antecedent streamflow
	Percentage area covered by shrub	Water temperature
	Percentage area made up of roads	Soil moisture root
	Percentage cropping area	Soil moisture deep
	Average soil TP content	
FRP	Percentage area covered by shrub	Same-day streamflow
	Percentage cropping area	Water temperature
	Catchment area	Soil moisture deep
	Average soil TP content	
	Mean channel slope	
TKN	Percentage clay area	Same-day streamflow
	Warmest quarter mean temperature	30-day antecedent streamflow
	Coldest quarter rainfall	NDVI
	Percentage cropping area	Water temperature
	Percentage pasture area	Soil moisture root
	Average soil TP content	Soil moisture deep
NO_x	Annual radiation	Same-day streamflow
	Warm quarter rainfall	30-day antecedent streamflow
	Hottest month maximum temperature	NDVI
	Average soil TP content	Water temperature
	Mean channel slope	Soil moisture root
		Soil moisture deep
EC	Annual radiation	Same-day streamflow
	Annual rainfall	14-day antecedent streamflow
	Wettest quarter rain	Water temperature
	Hottest month maximum temperature	Soil moisture root
	Percentage agriculture area	Soil moisture deep
	Percentage cropping area	
	Percentage area covered by shrub	
	Average soil TN content	

Table 2. The key catchment landscape characteristics that are related to the varying relationships of water quality and same-day streamflow across space, which were selected as the two predictors for the streamflow effect in our model. Two characteristics were selected to summary the variability of streamflow effects across space for each constituent, see Section 2.3 for details of the selection method. The corresponding Spearman's correlation (R, at $p<0.05$) between the effect of streamflow and each catchment characteristic is presented.

Constituent	Key factors that affect spatial variability in temporal effects	Spearman's ρ ($p<0.05$)
TSS	Annual rainfall	0.722
	Hottest month maximum temperature	-0.575
TP	Annual rainfall	0.695
	Percentage area used for cropping	-0.556
FRP	Percentage agriculture area	0.392
	Percentage area underlain by mixed igneous bedrock	0.314
TKN	Annual rainfall	0.713
	Hottest month maximum temperature	-0.618
NO_x	Total storage capacity of dams in catchment	-0.493
	Mean soil TN content	0.458
EC	Percentage area covered by grassland	-0.347
	Percentage area covered by woodland	-0.317

Table 3. Comparison of model performance for all records and only the above-DL records for each constituent.

Constituent	Above-DL records only	All records
TSS	0.225	0.397
TP	0.433	0.445
FRP	-1.920	0.199
TKN	0.658	0.630
NO_x	0.216	0.382
EC	0.907	0.886

Table 4. Model ability to capture observed water quality trends across all monitoring sites for each constituent. The percentages of sites where observed positive and negative trends are captured by the model are presented separately. Values in brackets indicate numbers of sites where corresponding positive or negative trends are observed. For detailed estimation of these percentages please refer to Sect. 2.2.

Constituent	% positive trends captured	% negative trends captured
TSS	33.3 (12)	85.0 (20)
TP	82.1 (28)	16.7 (12)
FRP	47.1 (17)	55.6 (9)
TKN	81.1 (37)	40.0 (10)
NO_x	68.6 (35)	66.7 (27)
EC	82.6 (23)	77.3 (22)

Table 5. Comparison of model performances (as NSE) of the full model (Column 2) and the 50 partial models (Columns 3 to 5) with each calibrated to 80% randomly selected monitoring sites. Columns 3 to 5 summarize the mean, minimum and maximum NSE values across the 50 runs, where for each constituent, the top row showing calibration performance and the bottom row showing the validation performance (i.e. at the 20% sites that were not used for calibration).

Constituent	Full model	50 CV mean	50 CV min	50 CV max
TSS	~~0.225~~0.397	0.413	0.376	0.439
		0.382	0.292	0.513
TP	~~0.433~~0.445	0.461	0.427	0.501
		0.411	0.151	0.575
FRP	~~-1.92~~0.199	0.168	0.067	0.232
		0.129	-0.078	0.272
TKN	~~0.658~~0.630	0.654	0.622	0.670
		0.622	0.468	0.691
NO_x	~~0.216~~0.382	0.453	0.414	0.489
		0.397	0.258	0.563
EC	~~0.907~~0.886	0.893	0.882	0.903
		0.875	0.809	0.924

Table 6~~3~~. Comparison of model performances (as NSE) of the full model and the three models that were calibrated to the pre-drought (1994-1996), drought (1997-2009) and the post-drought (2010-2014) periods. For each of the models, the calibration performance is shown on the top row and the validation performance (i.e. over the periods that were not used for calibration) is shown on the bottom row.

Constituent	Full model	Pre-drought calibration	During drought calibration	Post-drought calibration
TSS	0.397~~0.225~~	0.495	0.399	0.499

		0.208	0.402	0.390
TP	0.4450.433	0.477	0.438	0.525
		0.421	0.474	0.411
FRP	0.199-1.92	-1.336	0.187	0.204
		-1.406	0.197	0.024
TKN	0.6300.658	0.649	0.650	0.711
		0.566	0.648	0.610
NOx	0.3820.216	0.443	0.426	0.509
		0.394	0.471	0.393
EC	0.8860.907	0.854	0.901	0.901
		0.887	0.873	0.884

1003

Supplementary Materials

Table S1. Data sources of the potential spatial predictors for water quality (i.e. catchment characteristics). See Lintern et al. (2018b) for details.

	Catchment characteristic	Data Source
Climate	Average annual radiation (MJ $m^{-2}day^{-1}$)	(Geoscience Australia, 2011)
	Average temperature (°C)	(Geoscience Australia, 2011)
	Average temperature of warmest quarter (°C)	(Geoscience Australia, 2011)
	Average temperature of coldest quarter (°C)	(Geoscience Australia, 2011)
	Maximum temperature of hottest month (°C)	(Geoscience Australia, 2011)
	Minimum temperature of coldest month (°C)	(Geoscience Australia, 2011)
	Annual average rainfall (mm)	(Geoscience Australia, 2011)
	Average rainfall of the wettest quarter (mm)	(Geoscience Australia, 2011)
	Average rainfall of the driest quarter (mm)	(Geoscience Australia, 2011)
	Average rainfall of the coldest quarter (mm)	(Geoscience Australia, 2011)
	Average rainfall of the warmest quarter (mm)	(Geoscience Australia, 2011)
	Annual average catchment rainfall erosivity (MJ $mm^{-1}ha^{-1}hr^{-1}yr^{-1}$)	(Geoscience Australia, 2011)
Hydrology	Average annual runoff (mm)	(Geoscience Australia, 2011)
	Average of average daily flow (ML d^{-1})	Calculated using instantaneous flows from DELWP (2016)
	Standard deviation of average daily flow (ML d^{-1})	Calculated using instantaneous flows from DELWP (2016)
	Pereniality of runoff (%) (proportion of "contribution to mean annual discharge by the driest six months of the year" (Geoscience Australia, 2011))	(Geoscience Australia, 2011)
	Mean number of days where there is no flow annually (days $year^{-1}$)	Calculated using daily flows from DELWP (2016)
	Mean 7-day low flow (ML d^{-1})	Calculated using instantaneous flows from DELWP (2016)
	Mean Base Flow Index	Calculated using method outlined in Grayson et al. (1996)
	Maximum distance upstream to dam wall or reservoir (km)	(Geoscience Australia, 2011)
	Area of catchment comprised of farm dams (%)	(Department of Environment Land Water and Planning Victoria, 2016)
	Total storage capacity of dams in catchment normalized to average daily flow (ML $ML^{-1}d^{-1}$)	(Geoscience Australia, 2004)
Land use	Area of catchment urbanized (%)	(Bureau of Rural Sciences, 2010)
	Area of catchment made up of roads (%)	(Bureau of Rural Sciences, 2010)
	Area of catchment used for horticulture (%)	(Bureau of Rural Sciences, 2010)
	Area of catchment used for agriculture (%)[1]	(Bureau of Rural Sciences, 2010)
	Area of catchment used for pastures (grazing) (%)	(Bureau of Rural Sciences, 2010)
	Area of catchment used for cropping (%)[2]	(Bureau of Rural Sciences, 2010)
Land cover	Mean width of vegetated riparian zone (m)	(Department of Environment Land Water and Planning, 2014)
	Average fragmentation of riparian zone (%)	(Department of Environment Land Water and Planning, 2014)
	Area of catchment covered with grass (%)[3]	(Geoscience Australia, 2011)
	Area of catchment covered with forest (%)[4]	(Geoscience Australia, 2011)
	Area of catchment covered with shrubs (%)[5]	(Geoscience Australia, 2011)
	Area of catchment covered with woodland (%)[6]	(Geoscience Australia, 2011)
	Area of catchment bare (%)	(Geoscience Australia, 2011)

Soil type and geology	Area of catchment underlain by unconsolidated bedrock (%)	(Geoscience Australia, 2011)
	Area of catchment underlain by igneous bedrock (%)	(Geoscience Australia, 2011)
	Area of catchment underlain by sedimentary bedrock (%)	(Geoscience Australia, 2011)
	Area of catchment underlain by mixed igneous and sedimentary bedrock (%)	(Geoscience Australia, 2011)
	Average soil TP content (mg kg^{-1})	(Terrestrial Ecosystem Research Network, 2016)
	Average soil TN content (mg kg^{-1})	(Terrestrial Ecosystem Research Network, 2016)
	Average soil clay content (%)	(Terrestrial Ecosystem Research Network, 2016)
	Area of catchment with saline aquifers (%)	(Department of Agriculture and Water Resources, 2013)
Topography	Catchment area ($km^{2)}$	(Geoscience Australia, 2011)
	Mean catchment elevation (m)	(Geoscience Australia, 2011)
	Maximum catchment elevation (m)	(Geoscience Australia, 2011)
	Area of catchment made up of valley bottoms (%)	(Geoscience Australia, 2011)
	Total catchment length (km)	(Geoscience Australia, 2011)
	Mean catchment slope (%)	(Geoscience Australia, 2011)
	Mean channel slope (%)	Calculated using BOM (2012)

1. Agricultural activities include all primary production activities including plantation forests, grazing pastures, cropping and horticulture. This includes both dryland and irrigation agricultural activities.

2. Cropping refers to the production of commodities such as cereals, beverage and spice crops, hay, oilseeds, sugar, cotton, alkaloid poppies and pulses.

3. Grass refers to grasslands with tussock, hummock, reeds/rushes.

4. Forest refers to rainforests, Eucalypt forests, mangroves and low closed forests (e.g., Acacia, Melaleuca or Banksia species). Areas with high density of vegetation (>30% cover) and tall trees (>10 m).

5. Shrubs refers to open and dry woodlands and shrublands with hummock or tussock grass, Melaleuca shrublands, lignum shrublands, saltbush and chenopods. Areas with vegetation <2 m tall.

6. Woodlands refer to areas with medium trees (<10 m) at medium density (<30% cover).

Table S2. Data sources of the potential temporal predictors for water quality. See Guo et al. (2019) for details.

Data		**Source**
Daily rainfall (mm)		Australian Water Availability Project (AWAP) (Raupach et al., 2009, 2012) Available from: http://www.csiro.au/awap; http://www.bom.gov.au/jsp/awap/index.jsp
Daily average temperature (°C)		
Daily actual ET (mm)		Australian Water Resources Assessment (Frost et al., 2016) Available from: http://www.bom.gov.au/water/landscape
Daily average root zone soil moisture		
Daily average deep soil moisture		
Monthly NDVI	January 1994 – December 1999	Advanced Very High Resolution Radiometer product (AVHRR) (Eidenshink, 1992) Available from: https://earthdata.nasa.gov/
	January 2000 – December 2013	Moderate Resolution Imaging Spectroradiometer (MODIS); MOD13A3 (NASA LP DAAC, 2017) Available from: https://earthdata.nasa.gov/

Table S3. Log-sinh transformation parameter (a and b) values for 50 potential spatial predictors for stream water quality (i.e. catchment characteristics).

Catchment characteristics	***a***	***b***
Annual radiation (MJ $m^{-2}day^{-1}$)	3.458	2.052
Annual temperature (°C)	2.425	3.133
Annual rainfall (mm)	0.008	0.001
Erosivity (MJ $mm^{-1}ha^{-1}hr^{-1}yr^{-1}$)	0.030	0.000
Driest quarter rain (mm)	0.099	0.003
Wettest quarter rain (mm)	0.002	0.003
Warmest quarter rainfall (mm)	0.039	0.005
Coldest quarter rainfall (mm)	0.001	0.001
Coldest month minimum temperature (°C)	4.999	0.000
Hottest month maximum temperature (°C)	0.000	0.002
Coldest quarter mean temperature (°C)	4.986	4.996
Warmest quarter mean temperature (°C)	3.805	2.193
Average of average daily flow (ML d^{-1})	0.002	0.001
Average of average daily flow (ML d^{-1})	0.034	0.002
Standard deviation of average daily flow (ML d^{-1})	0.012	0.430
Pereniality of runoff (%) (proportion of 'contribution to mean annual discharge by the driest six months of the year'	0.106	0.152
Mean number of days where there is no flow annually (days $year^{-1}$)	0.000	0.066
Mean 7-day low flow (ML d^{-1})	0.045	3.319
Mean Base Flow Index	4.896	0.000
Maximum distance upstream to dam wall or reservoir (km)	0.034	0.006
Area of catchment comprised of farm dams (%)	0.000	5.000
Total storage capacity of dams in catchment normalized to average daily flow (ML $ML^{-1}d^{-1}$)	0.003	0.002
Area of catchment urbanized (%)	0.000	0.135
Area of catchment made up of roads (%)	0.055	0.729
Area of catchment used for agriculture (%)	4.998	4.995
Area of catchment used for pastures (grazing) (%)	0.174	0.114
Area of catchment used for cropping (%)	0.000	0.079
Area of catchment used for horticulture (%)	0.000	0.373
Mean width of vegetated riparian zone (m)	0.293	0.013
Average fragmentation of riparian zone (%)	0.174	0.132
Area of catchment covered with grass (%)	0.000	0.158
Area of catchment covered with forest (%)	0.238	0.020
Area of catchment covered with shrubs (%)	0.000	0.403
Area of catchment covered with woodland (%)	0.002	0.108
Area of catchment bare (%)	0.000	5.000
Area of catchment underlain by unconsolidated bedrock (%)	0.024	0.050
Area of catchment underlain by igneous bedrock (%)	0.034	0.068
Area of catchment underlain by sedimentary bedrock (%)	4.998	4.995
Area of catchment underlain by mixed igneous and sedimentary bedrock (%)	0.000	0.032
Average soil TP content (mg kg^{-1})	0.044	4.744
Average soil TN content (mg kg^{-1})	0.213	1.733

Average soil clay content (%)	0.000	0.021
Area of catchment with saline aquifers (%)	0.001	0.000
Catchment area (km^2)	0.177	0.001
Mean catchment elevation (m)	0.044	0.001
Area of catchment made up of valley bottoms (%)	0.002	0.074
Total catchment length (km)	0.003	0.001
Mean catchment slope (%)	0.078	0.068
Mean channel slope (%)	0.029	4.899
Average soil clay content (%)	0.103	0.040

Table S4. Box-Cox transformation parameter (λ) values for the six water quality constituents and the nineteen potential temporal predictors. Values in bracket show the standard deviation of individual site-level λ.

Water Quality Constituent	**λ**
TSS	-0.249 (0.287)
TP	-0.058 (0.181)
FRP	-0.836 (1.056)
TKN	0.141 (0.342)
NO_x	0.107 (0.305)
EC	-0.024 (0.921)
Temporal predictors	**λ**
Rainfall (mm)	0.106 (0.041)
Rainfall on previous day (mm)	0.108 (0.028)
Averaged rainfall over previous 3 days (mm)	0.157 (0.022)
Averaged rainfall over previous 7 days (mm)	0.220 (0.025)
Averaged rainfall over previous 14 days (mm)	0.192 (0.046)
Averaged rainfall over previous 30 days (mm)	0.116 (0.075)
Streamflow (mm d^{-1})	-0.015 (0.225)
Streamflow on previous day (mm d^{-1})	-0.027 (0.207)
Averaged Streamflow over previous 3 days (mm d^{-1})	-0.032 (0.207)
Averaged Streamflow over previous 7 days (mm d^{-1})	-0.030 (0.2)
Averaged Streamflow over previous 14 days (mm d^{-1})	-0.021 (0.198)
Averaged Streamflow over previous 30 days (mm d^{-1})	-0.004 (0.195)
Dry spell length in the past 14 days (days)	0.257 (0.089)
NDVI for the month	3.715 (1.998)
Water temperature (°C)	0.357 (0.269)
Air temperature (°C)	0.231 (0.244)
Evaporation (mm)	0.019 (0.13)
Root zone soil moisture (%)	0.913 (0.648)
Deep soil moisture (%)	0.357 (0.269)

Table S5. The key temporal predictor for each water quality constituent, and the two key factors that are mostly closely related to the spatial variation of each temporal predictor (see Section 2.3 in the main text for detailed selection process). The corresponding Spearman's correlation coefficients (R) are also shown in the last column.

Constituent	**Key factors that affect temporal variability**	**Key factors that affect spatial variability in temporal effects**	**Spearman's R**
TSS	Same-day streamflow	Annual rainfall	0.722
		Hottest month maximum temperature	-0.575
	7-day antecedent streamflow	Annual runoff	-0.536

		Mean elevation	-0.465
	Water temperature	Daily flow standard deviation	0.204
		Total catchment length	0.177
	Soil moisture root	Percentage area with saline aquifers	0.507
		Hottest month maximum temperature	0.495
	Soil moisture deep	Maximum distance upstream to dam wall or reservoir	-0.275
		Percentage area covered by grassland	-0.24
TP	Same-day streamflow	Annual rainfall	0.695
		Hottest month maximum temperature	-0.556
	30-day antecedent streamflow	Erosivity	-0.675
		Percentage cropping area	0.626
	Water temperature	Percentage agricultural area	0.382
		Percentage area used for roads	0.274
	Soil moisture root	Percentage pasture area	0.564
		Hottest month maximum temperature	0.557
	Soil moisture deep	Percentage area underlain by mixed igneous bedrock	-0.23
		Maximum distance upstream to dam wall or reservoir	-0.21
FRP	Same-day streamflow	Percentage agriculture area	0.392
		Percentage area underlain by mixed igneous bedrock	0.314
	Water temperature	Total catchment length	-0.28
		Coldest quarter mean temperature	0.232
	Soil moisture deep	Percentage area used for roads	-0.21
		Percentage aea covered by woodland	0.204
TKN	Same-day streamflow	Annual rainfall	0.713
		Hottest month maximum temperature	-0.618
	30-day antecedent streamflow	Erosivity	-0.823
		Percentage cropping area	0.694
	NDVI	Mean_7daylowflow	0.42
		Maximum distance upstream to dam wall or reservoir	-0.366
	Water temperature	Coldest quarter rainfall	-0.386
		Maximum distance upstream to dam wall or reservoir	0.374
	Soil moisture root	Warmest quarter mean temperature	0.6
		Percentage pasture area	0.588
	Soil moisture deep	Hottest month maximum temperature	-0.274
		Warmest quarter mean temperature	-0.269
NOx	Same-day streamflow	Total storage capacity of dams in catchment	-0.493
		Mean soil TN content	0.458
	30-day antecedent streamflow	Coldest quarter rainfall	-0.413
		Hottest month maximum temperature	0.396
	NDVI	Percentage area covered by woodland	-0.442

		Maximum elevation	-0.428
	Water temperature	Percentage area underlain by mixed igneous bedrock	0.266
		Percentage urbanized area	-0.2
	Soil moisture root	Annual temperature	0.44
		Warmest quarter average temperature	0.338
	Soil moisture deep	Percentage horticulture area	0.341
		Wettest quarter rainfall	-0.334
EC	Same-day streamflow	Percentage area covered by grassland	-0.347
		Percentage area covered by woodland	-0.317
	14-day antecedent streamflow	Percentage area covered by forest	0.324
		PerForest_Ext	0.276
	Water temperature	Coldest month minimum temperature	-0.328
		Mean catchment slope	0.28
	Soil moisture root	Mean 7-day low flow	0.33
		Average soil TN content	0.303
	Soil moisture deep	Maximum elevation	0.366
		Percentage area covered by woodland	0.312

30

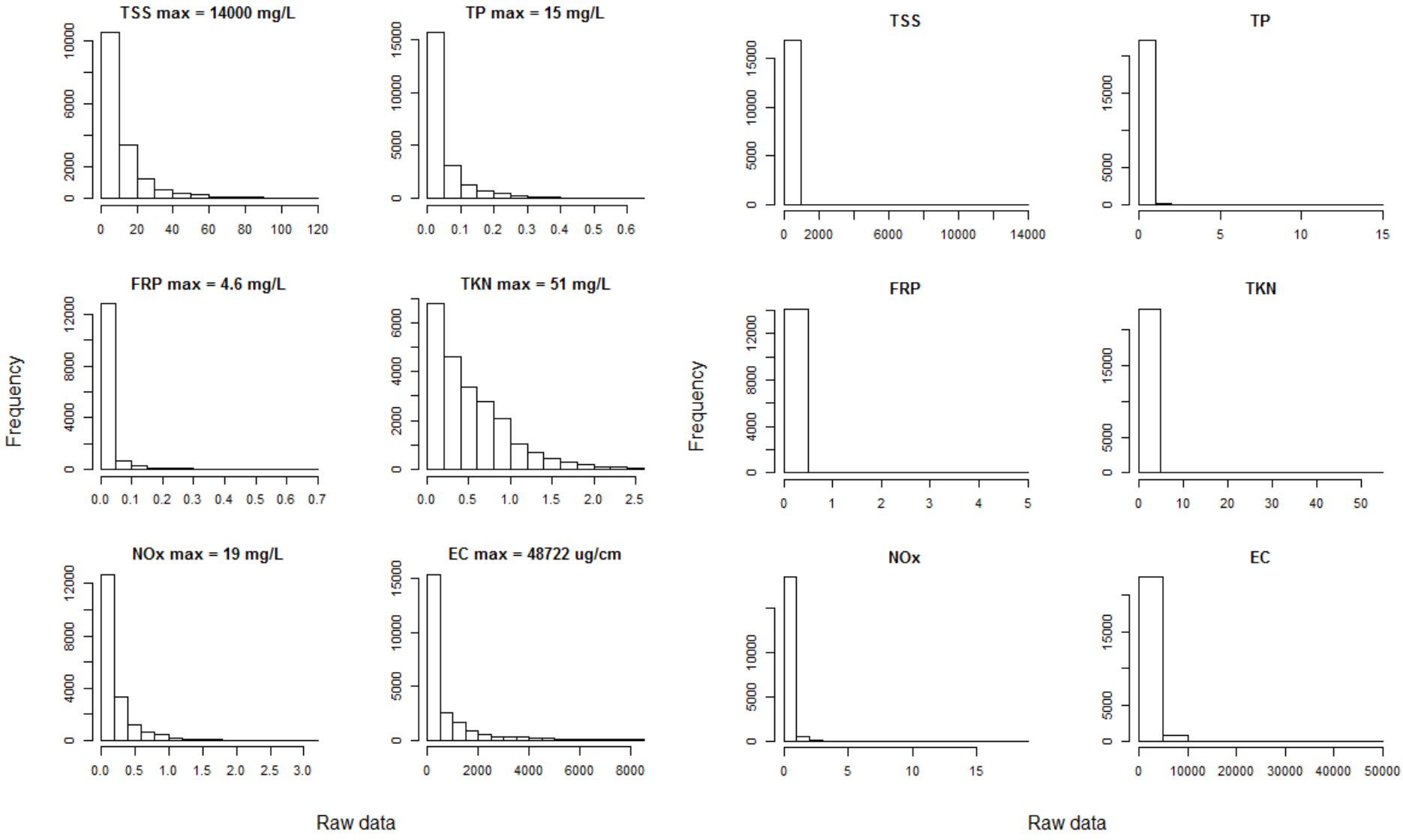

Figure S1. Distribution of the raw water quality data across all catchments. Each panel shows one constituent with only the above-DL data. To help visualizing the highly skewed data, the top percentile of data for each constituent were not plotted, while the maximum value was shown in text.

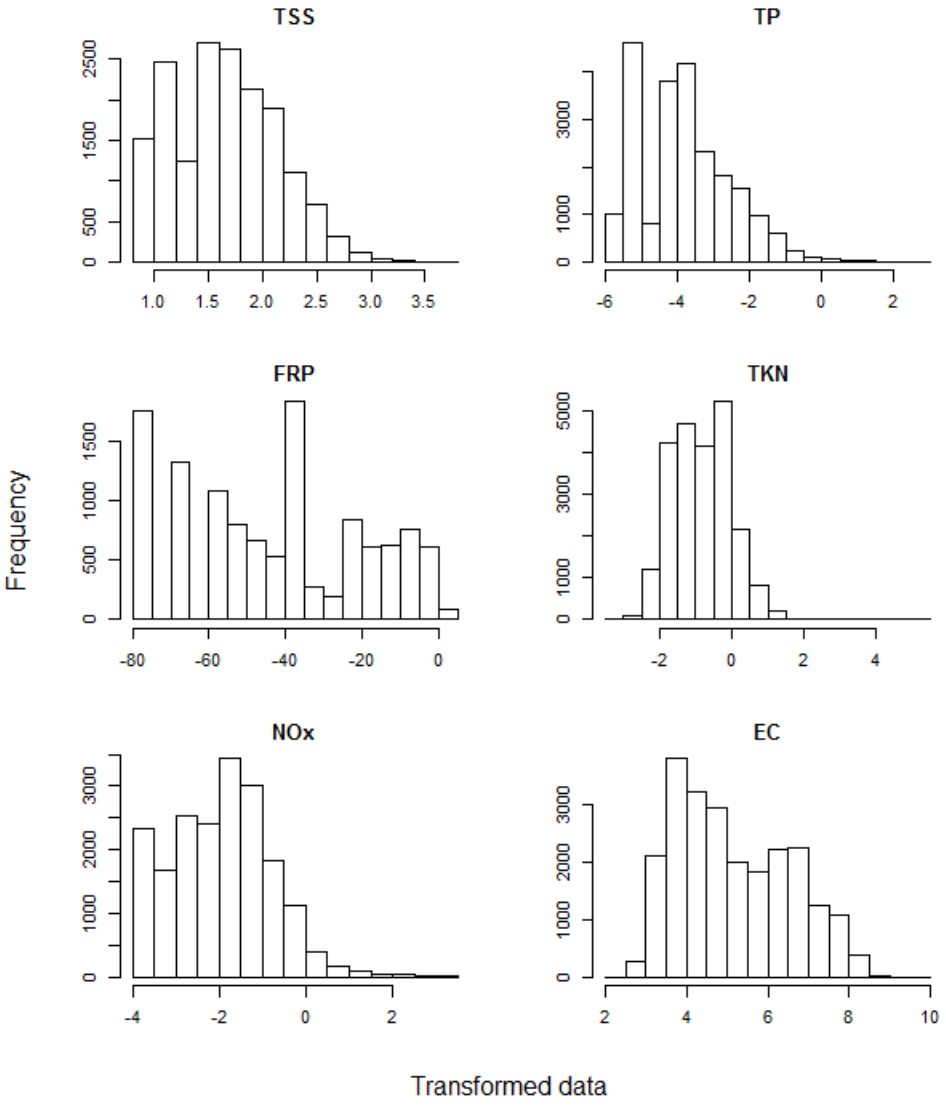

Figure S2. Distribution of the transformed water quality data across all catchments. Each panel shows one constituent with only the above-DL data.

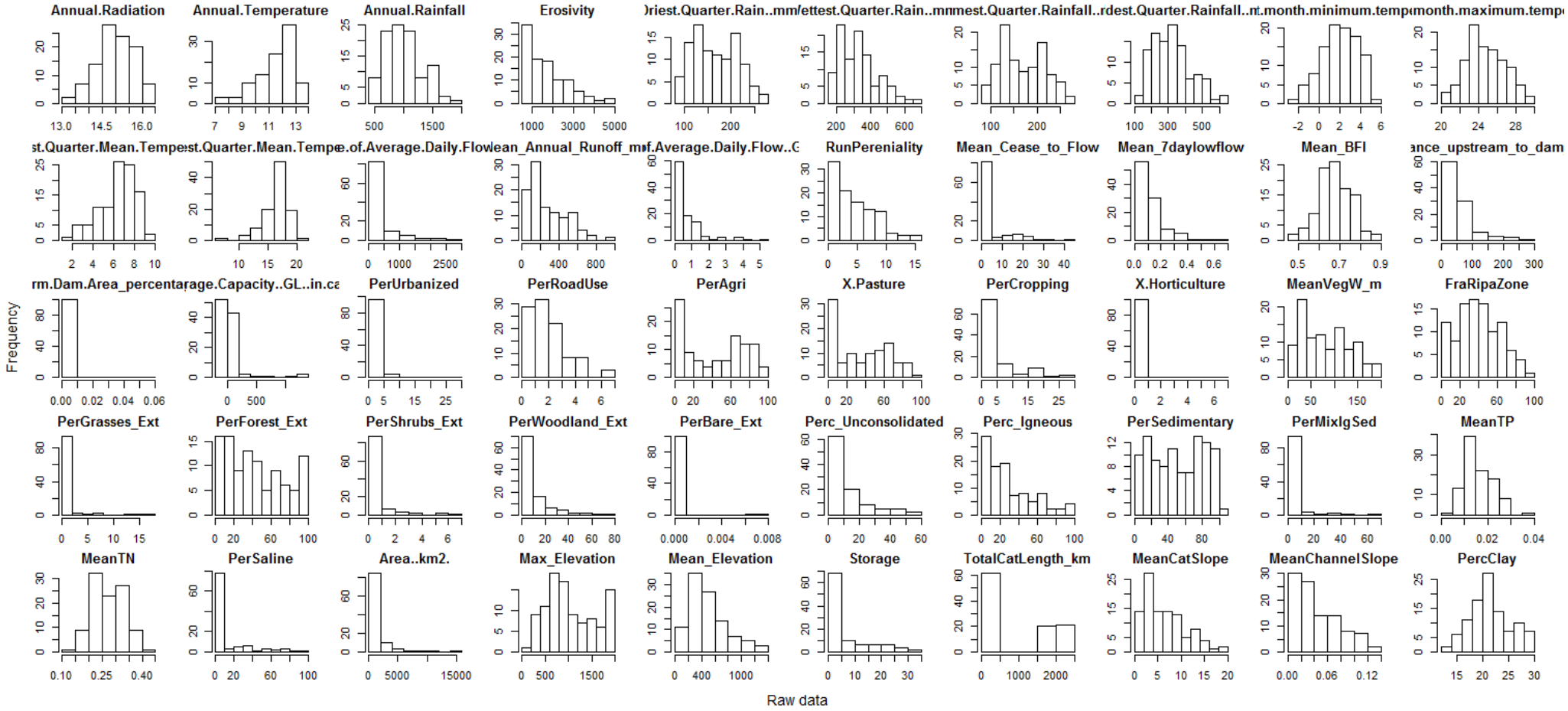

36

37 **Figure S3. Distribution of the raw data for catchment characteristics included as potential spatial predictors in the model.**

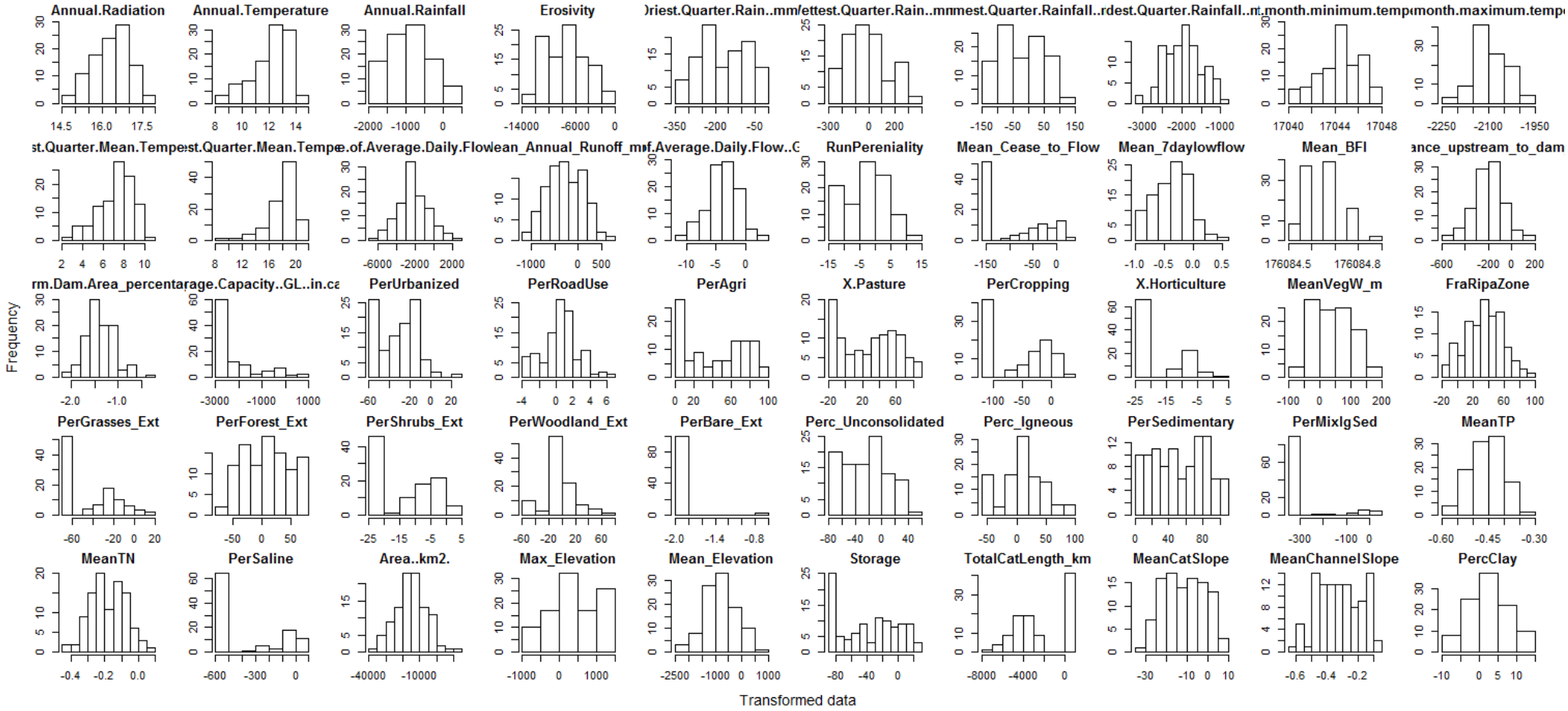

Figure S4. Distribution of the transformed data for catchment characteristics included as potential spatial predictors in the model.

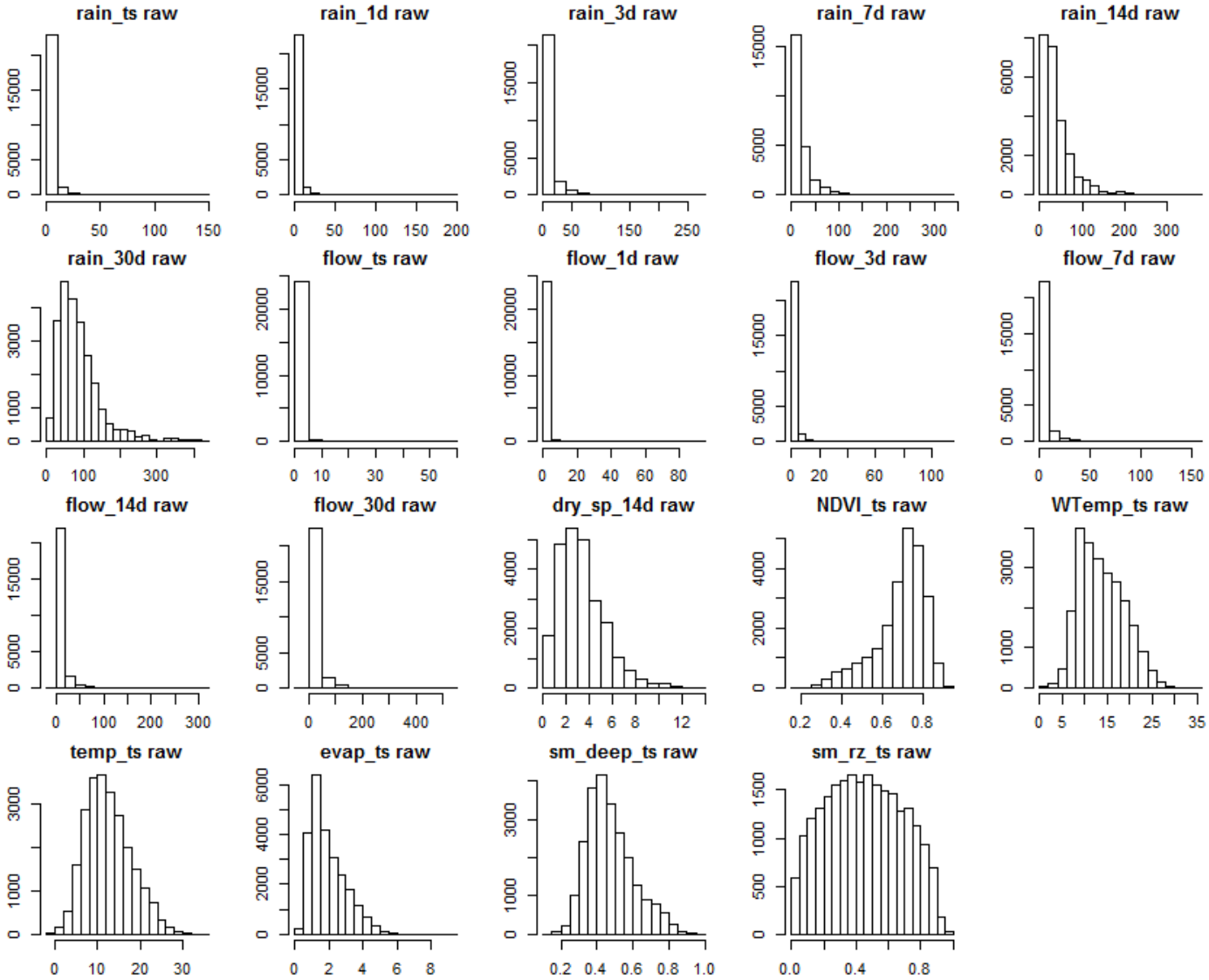

Figure S5. Distribution of the raw data for hydro-climatic and vegetation variables included as potential temporal predictors in the model.

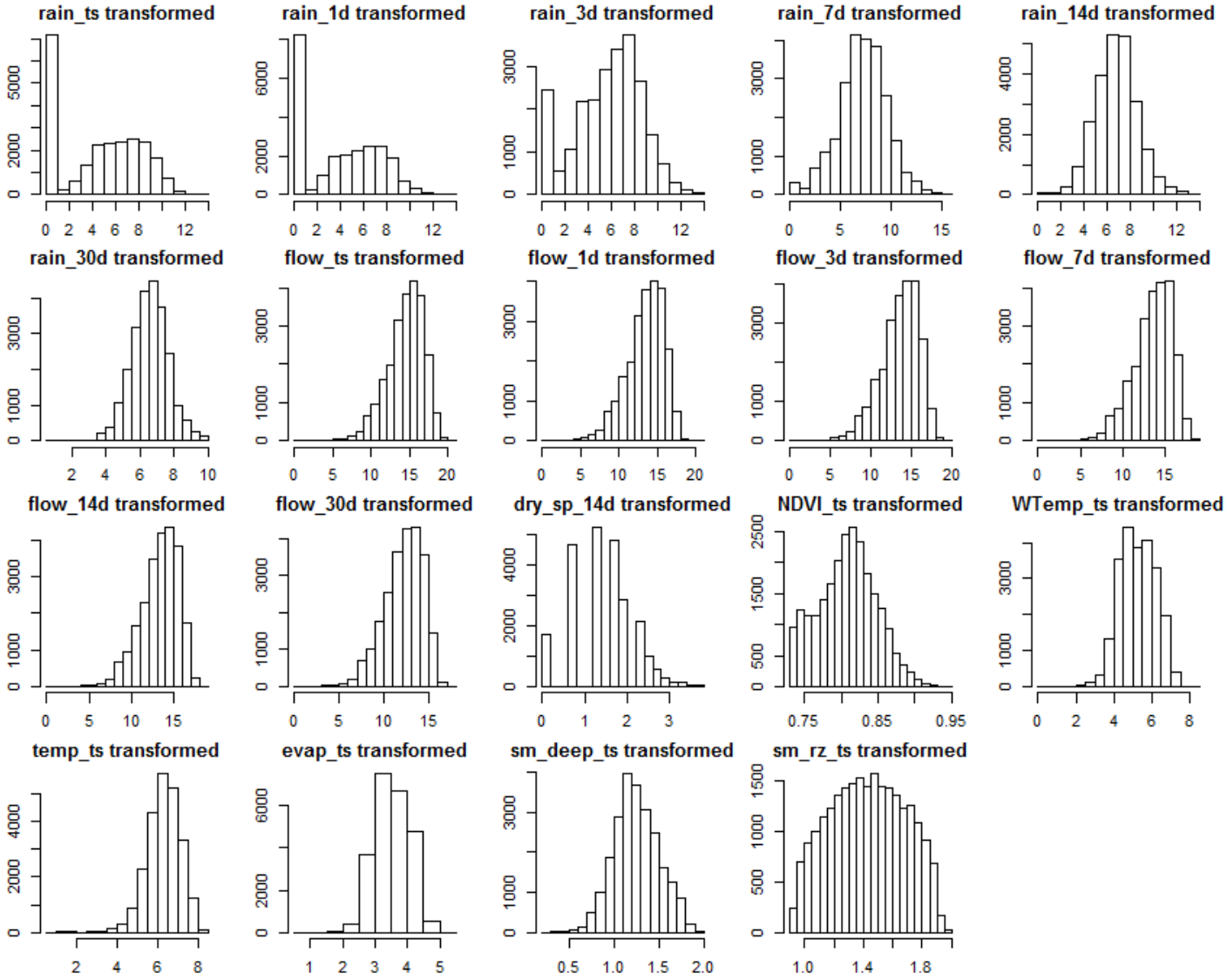

Figure S6. Distribution of the transformed data for transformed (Box-Cox) hydro-climatic and vegetation variables included as potential temporal predictors in the model.

Figure S4. The two key factors that are mostly closely related to the spatial variation of each temporal predictor of each water quality constituents, as highlighted in the coloured cells (see Section 2.3 in the main text for detailed selection of the two key factors). Colours indicate the corresponding Spearman's correlation coefficients (R) from -1 (red) to 1 (blue).

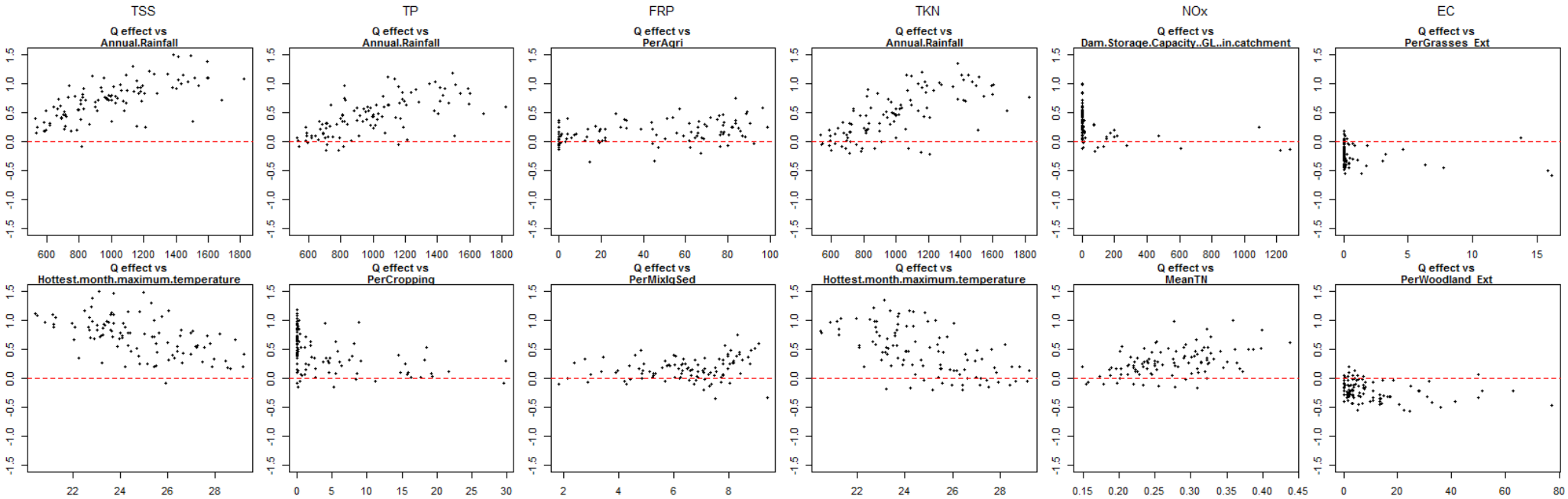

Figure S5. Effects of streamflow across catchments against the two most important catchment landscape characteristics, for each constituent (see Section 2.3 in the main text for detailed selection of the two key factors). Red dash lines indicate the zero levels, and thus differentiate positive and negative streamflow effects

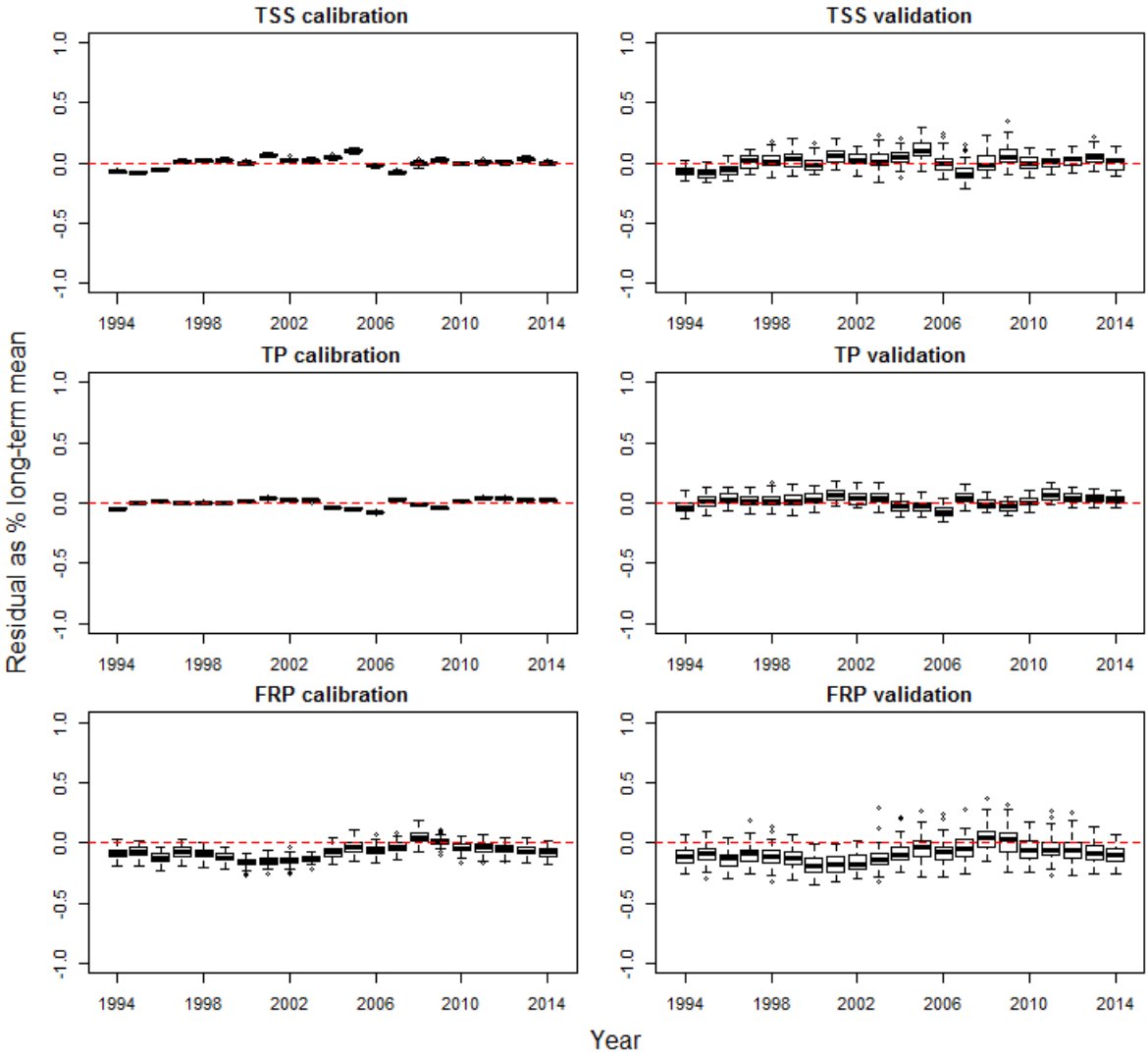

54

55 **Figure S6. Annual average residuals of the models for TSS, TP and FRP, as % of long-term average. All**
56 **values are presented in a Box-Cox transformed scale.**

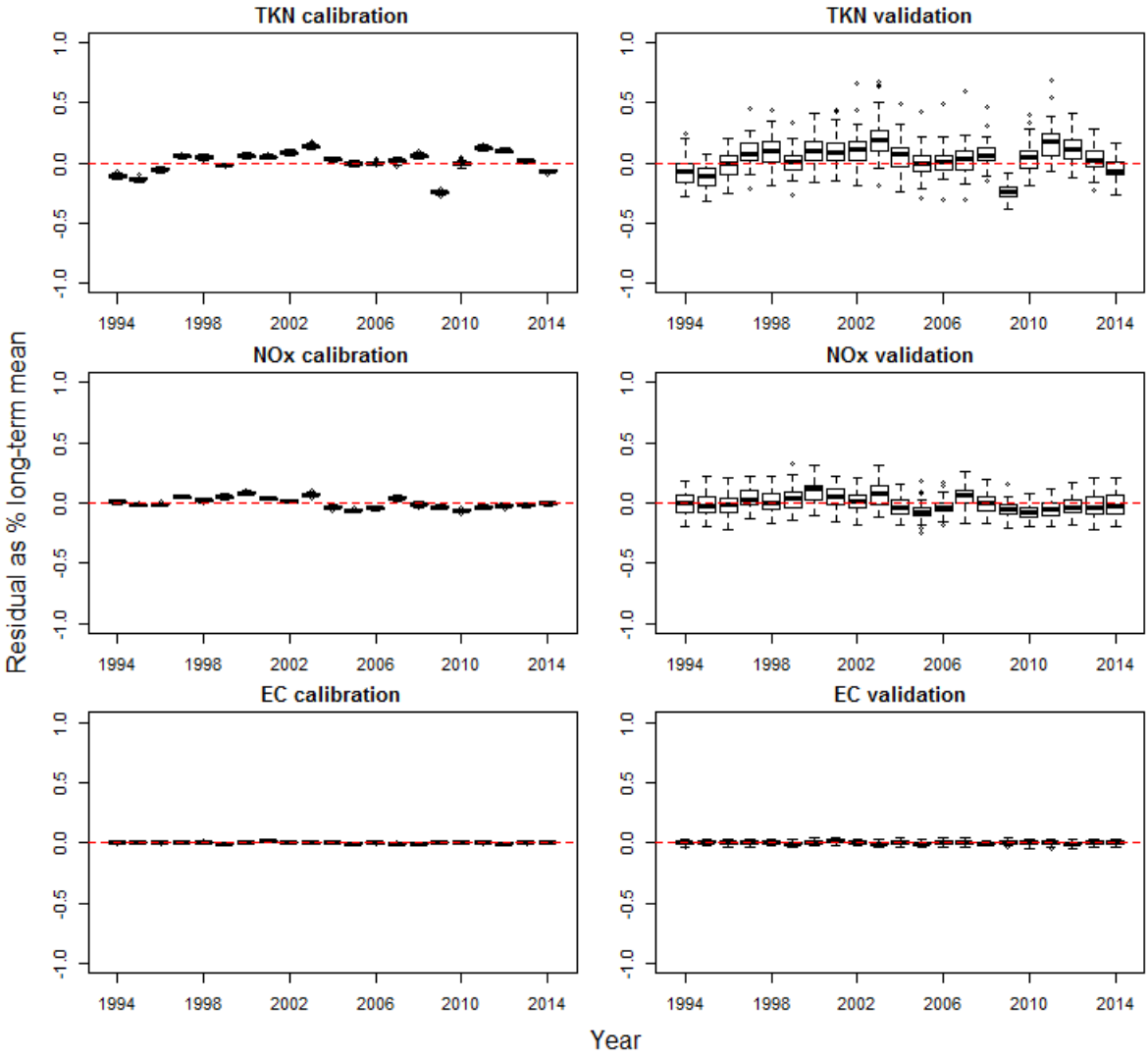

Figure S7. Annual average residuals of the models for TKN, NOx and EC, as % of long-term average. All values are presented in a Box-Cox transformed scale.

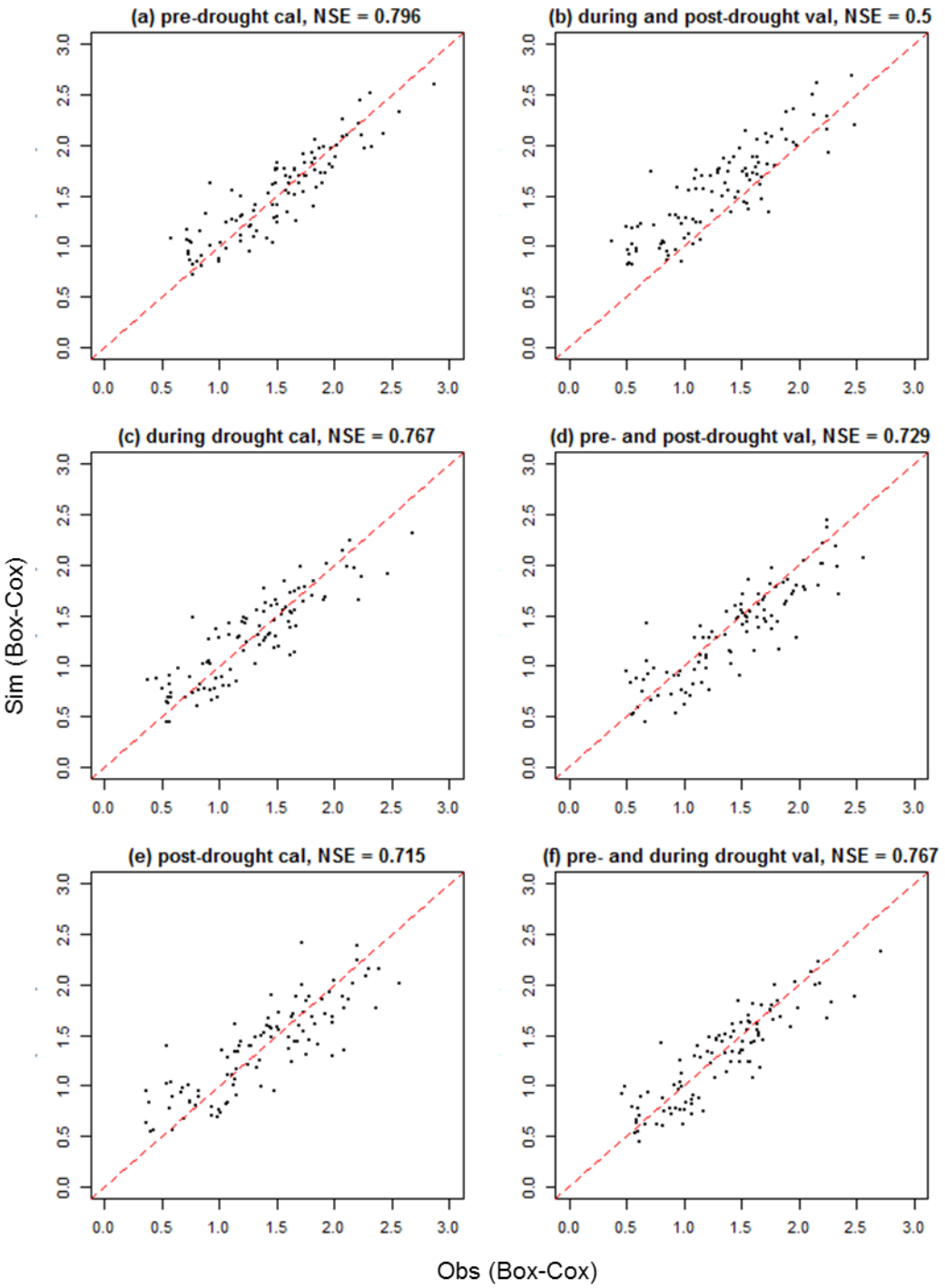

Figure S8. Comparison of the TSS model performance, as the simulated against observed site-level mean concentrations across three different calibration/validation periods for calibrations on the pre-drought (1994-1996), drought (1997-2009) and the post-drought (2010-2014) periods, respectively, see Section 2.4 for details of the calibration and validation approach.

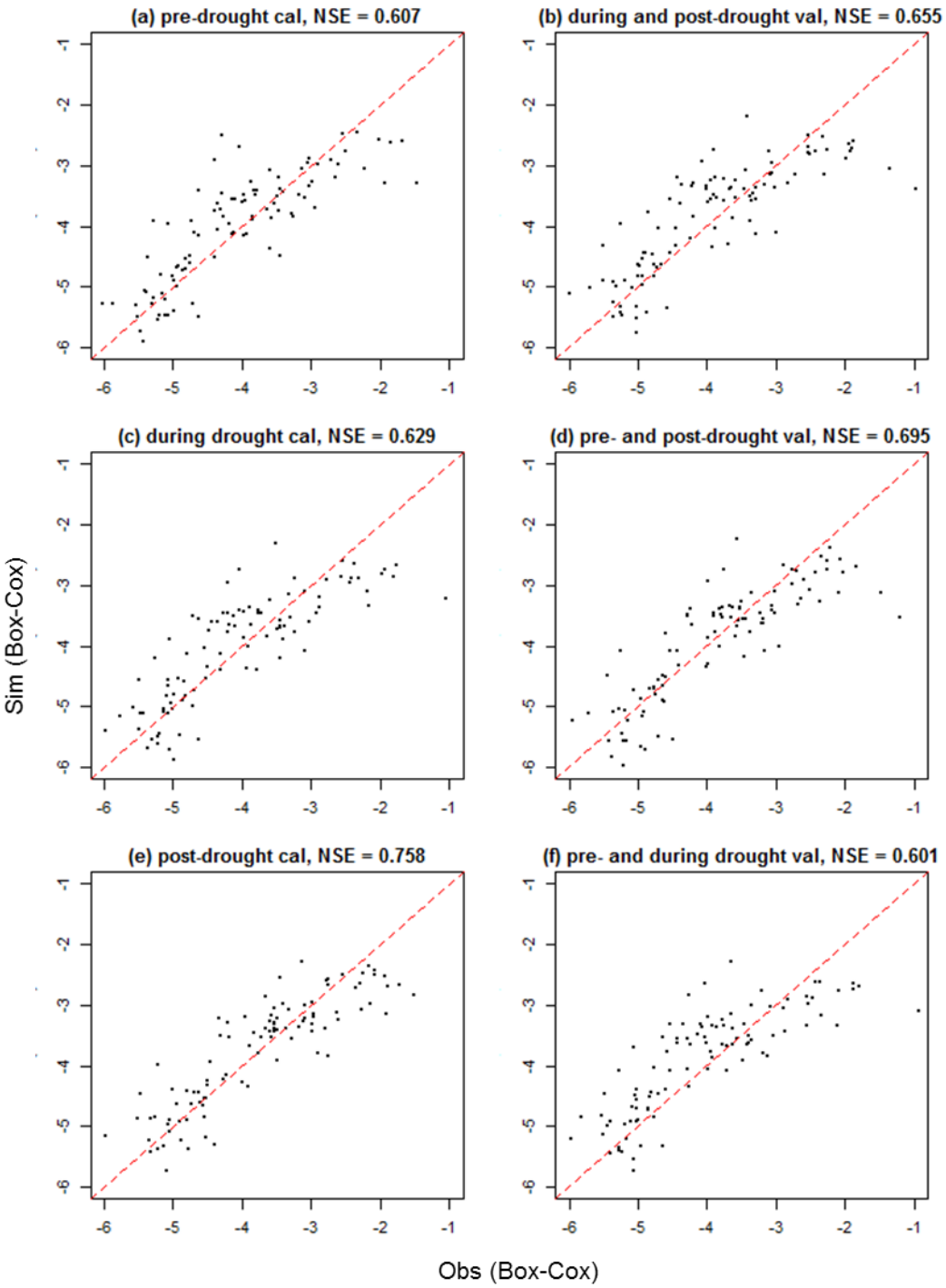

Figure S9. Comparison of the TP model performance, as the simulated against observed site-level mean concentrations across three different calibration/validation periods for calibrations on the pre-drought (1994-1996), drought (1997-2009) and the post-drought (2010-2014) periods, respectively, see Section 2.4 for details of the calibration and validation approach.

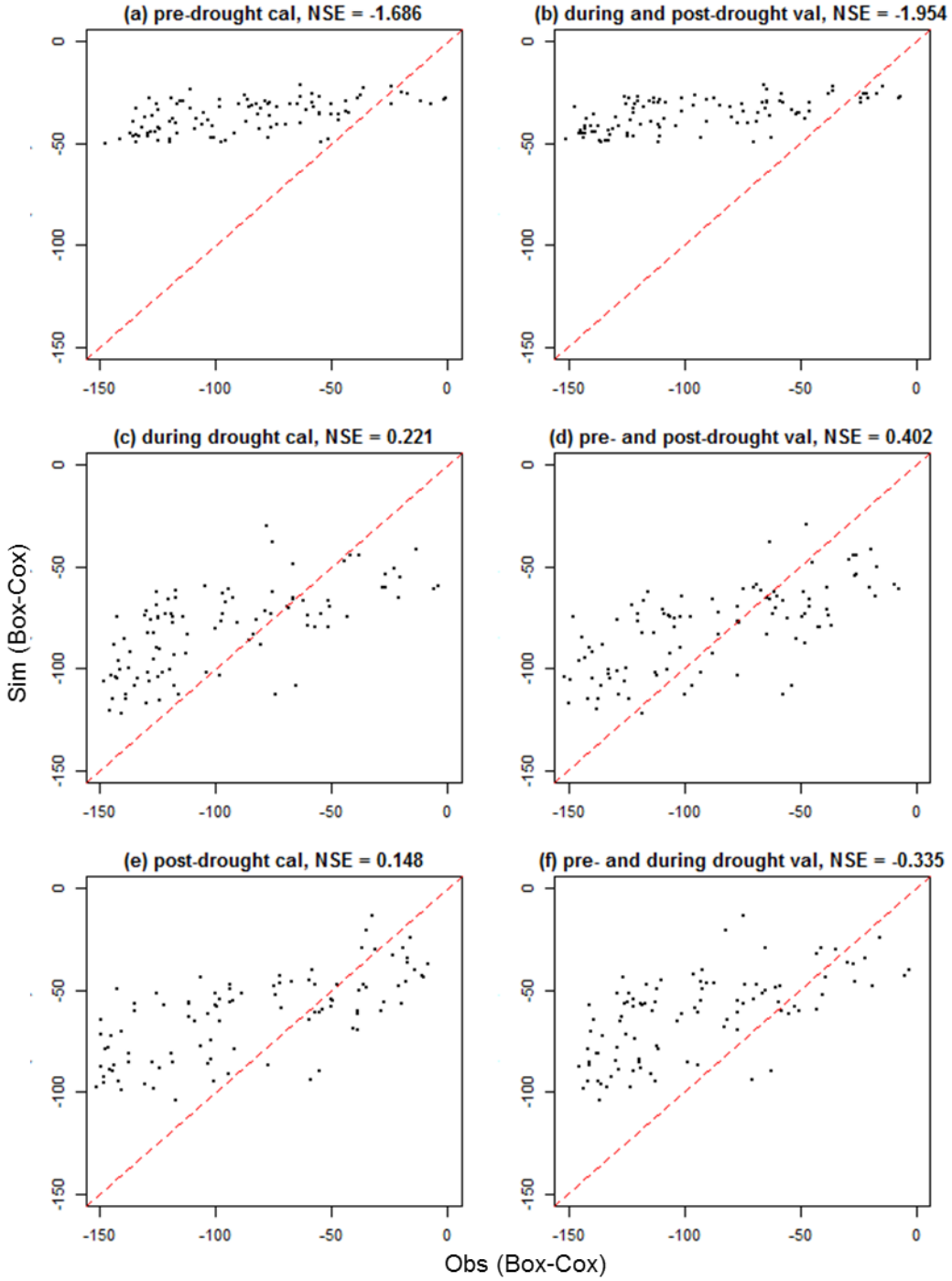

Figure S10. Comparison of the FRP model performance, as the simulated against observed site-level mean concentrations across three different calibration/validation periods for calibrations on the pre-drought (1994-1996), drought (1997-2009) and the post-drought (2010-2014) periods, respectively, see Section 2.4 for details of the calibration and validation approach. Note that the unstable performance can be resulted by the poor performance for the full model, see Section 3.1.

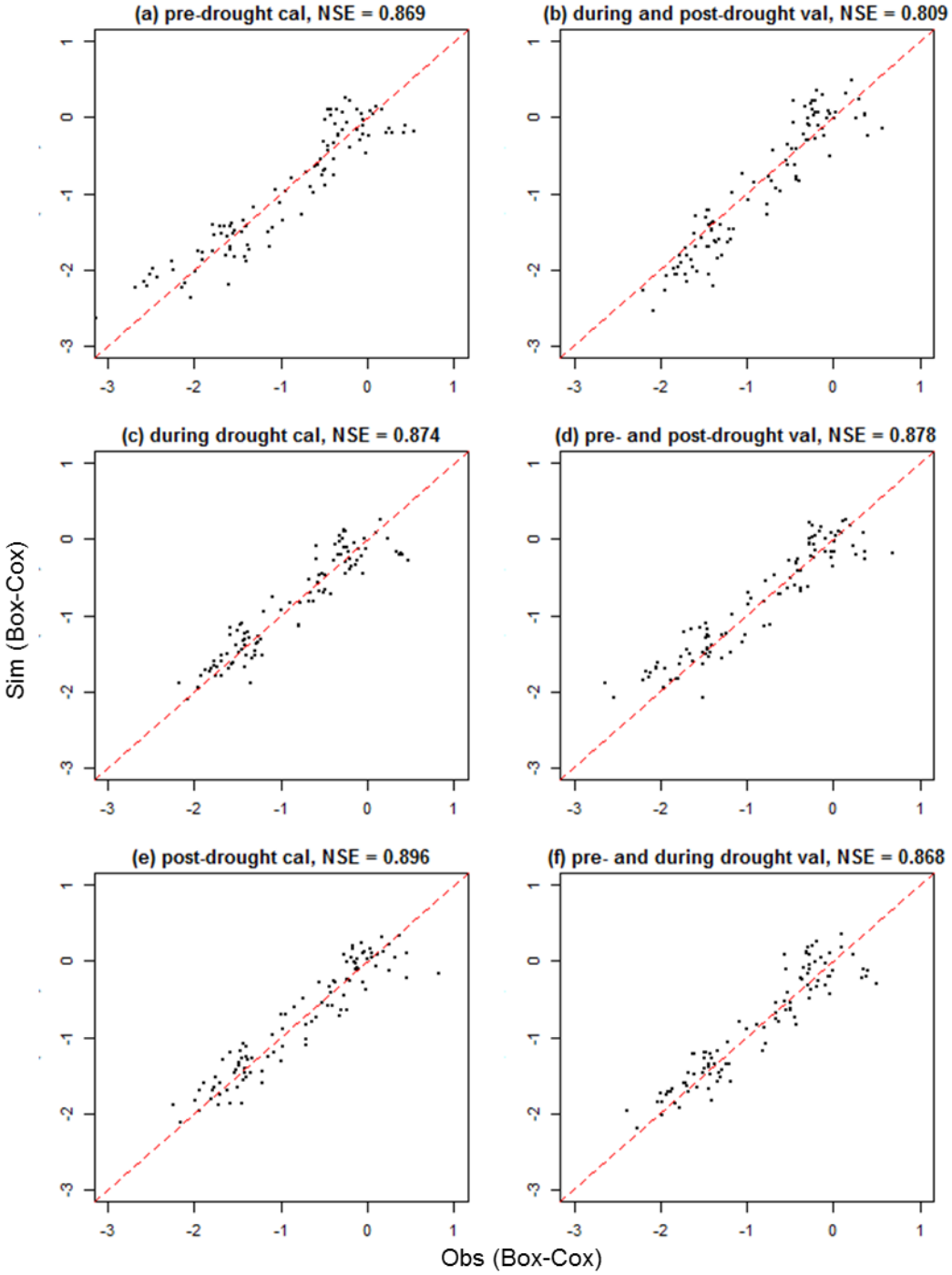

Figure S11. Comparison of the TKN model performance, as the simulated against observed site-level mean concentrations across three different calibration/validation periods for calibrations on the pre-drought (1994-1996), drought (1997-2009) and the post-drought (2010-2014) periods, respectively, see Section 2.4 for details of the calibration and validation approach.

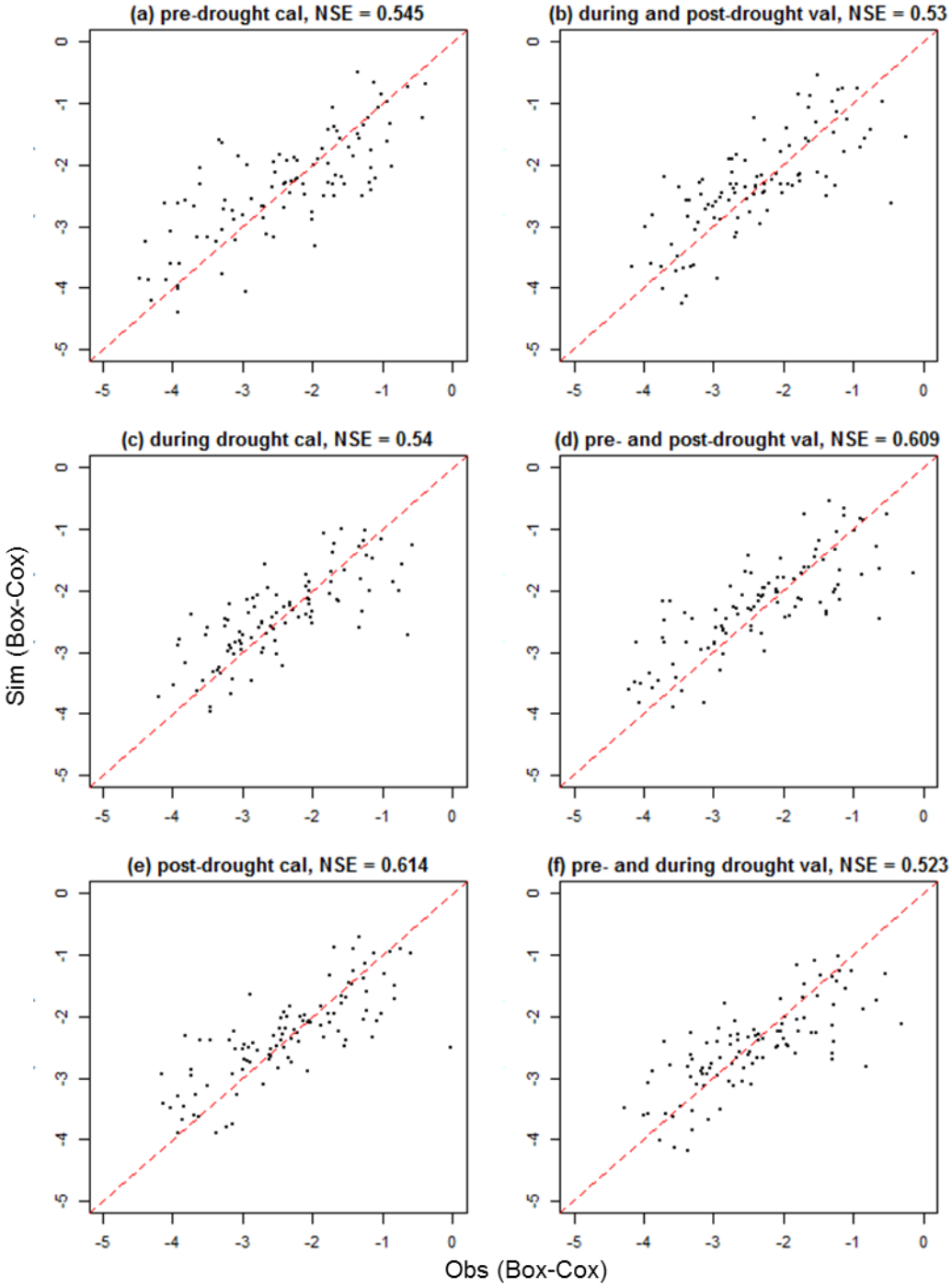

Figure S12. Comparison of the NO_x model performance, as the simulated against observed site-level mean concentrations across three different calibration/validation periods for calibrations on the pre-drought (1994-1996), drought (1997-2009) and the post-drought (2010-2014) periods, respectively, see Section 2.4 for details of the calibration and validation approach.

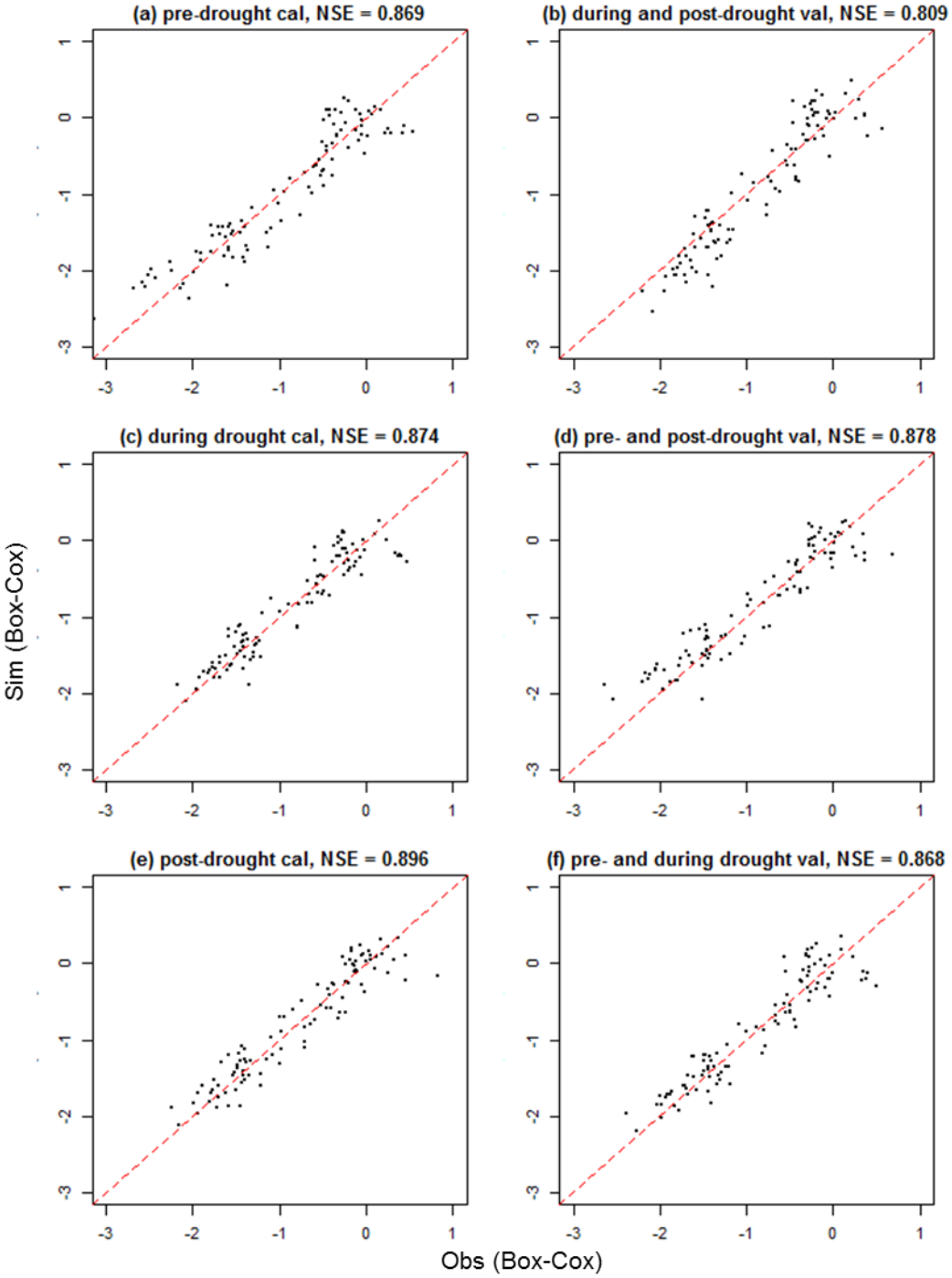

Figure S13. Comparison of the EC model performance, as the simulated against observed site-level mean concentrations across three different calibration/validation periods for calibrations on the pre-drought (1994-1996), drought (1997-2009) and the post-drought (2010-2014) periods, respectively, see Section 2.4 for details of the calibration and validation approach.

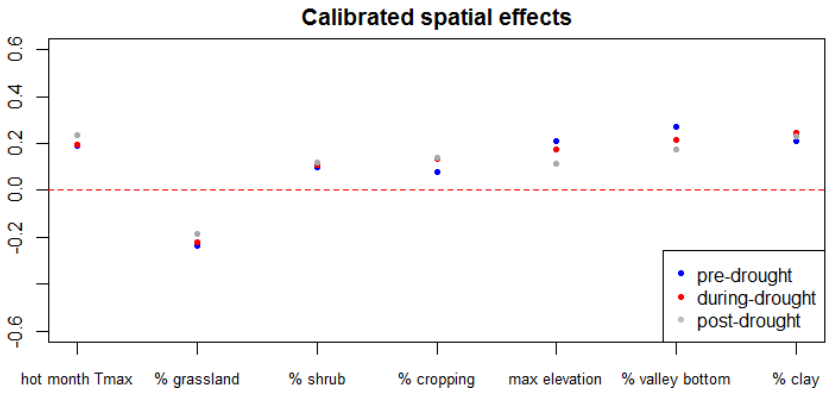

Figure S14. Effects of the seven key predictors for the spatial variability in TSS across 102 sites, summarized by the posterior mean of the calibrated parameter values for each predictor, to the pre-, during- and post-drought periods (differentiated by colour). The seven key predictors are, from left: hottest month maximum temperature, percentage catchment area as grassland, percentage catchment area as shrub, percentage catchment area as cropping land, maximum catchment elevation, percentage catchment area made up of valley bottoms, and average soil clay content.